Status Report for Experiment AD-4/ACE

Michael Holzscheiter[1,2], Jan Alsner[3], Angelo Angelopoulos[4], Niels Bassler[3,5], Gerd Beyer[6], Rebecca Boll[2], Massimo Caccia[7], Fred Currell[8], Michael Doser[9], Oliver Hartley[6], Oliver Jäkel[5], Ioannis Kantemiris[4], Franz Joachim Kaiser[5], Joy Kavanagh[7], Helge Knudsen[10], Roy Keyes[1], Søren Pape Møller[10], Loretta Negrini[7], Jens Overgaard[3], Jørgen Petersen[3], Osman Ratib[6], Hermann Rochus[4], Giuseppe Schettino[8], Stefan Sellner[2], Tina Straße[2], Sara Tegami[2], David Timson[8], Heikki Tölli[11], Brita Singers-Sørensen[3], Timothy Solberg[12], Carsten Welsch[2], Patrick Weber[9]

[1] University of New Mexico, [2]Max Planck Institute for Nuclear Physics, Heidelberg
[3]Aarhus University Hospital, [4] University of Athens,[5]Deutsches Krebsforschungszentrum
[6]Geneva University Hospital, [7] Universita d'Insubria, Como, [8]Queens University of Belfast ,
[9]CERN, [10]Aarhus University, [11]University of Umeå,
[12]University of Texas,

I. Introduction

The overall goal of the AD-4 Experiment is to study the biological effect of antiprotons in order to validate earlier theoretical predictions that antiprotons could produce a better therapeutic ratio for the treatment of well defined tumors. This prediction is based on three observations:

1. The physical dose should be augmented near the end of range due to the additional energy deposited locally when antiprotons annihilate.
2. Some of the additional energy deposited results from low energy heavy ion recoils produced in the annihilation event, which are expected to exhibit a higher biological efficiency.
3. Pions and high-energy photons generated in the annihilation events can be used to detect in real time the exact location of the treatment.

Progress in all these areas has been made in 2010 and is discussed in this report and the attached appendices.

This was the first year where we deviated from the one week/year run schedule and had requested and received an additional 5 shifts for detector development and commissioning of the changed set-up, necessitated by the rearrangement of the beam line in the DEM zone and the addition of new equipment for AEGIS to the zone. These extra shifts also took some of the time pressure off the biological measurement series, which allowed us to augment our existing data with a new complete data set.

Using our new beam monitor we noticed significant changes from shot to shot in shape (and occasional in position) of the beam, which before had gone unnoticed. While these fluctuations may have little effect on the other experiments, in our case the survival of the cells depends strongly on the exact dose distribution in a 6 mm diameter cylinder along the beam axis and knowledge of the shot by shot beam parameters is now being included in our final data analysis. This has not yet been completed and the data shown for this year still need to be calibrated in order to combine them with previous year's measurements.

II. Clonogenic Survival of V79 Chinese Hamster Cells

Overview

In 2006, 2007, 2008, 2009, and 2010 we were assigned 1 week each of antiproton beam time, using a special extraction method providing a beam of 502 MeV/c antiprotons. As this extraction method is sufficiently different from normal AD operation it was decided to lump all beam time into a single run of 7 days of 24 hours. Typically, 5 of these 7 days are dedicated to biological measurements.

The remaining 2 days are needed for beam set-up and also can be partially used beneficially for physics studies of dosimetry systems, beam monitors, and to collect dose data for Monte Carlo benchmarking, as can be the breaks in between different badges of cell samples due to the logistics of shipping viable cells with a survival time of only about 60 hours to CERN and back.

The 502 MeV/c antiproton beam from the AD provides a penetration into our target of approximately 10 cm. We use a set of passive degraders to generate a spread-out Bragg peak of 10 mm depth, irradiating a volume of approximately 300 mm^3. This allows a clear separation between the entrance channel, where we expect low LET (and thereby low RBE) to dominate from the high LET/RBE region around the end of range.

Figure 1 shows the raw data from the October 2008 data run where we achieve a Spread-Out Bragg Peak with a flat peak region. It can be seen that the sensitivity of the clonogenic assay allows to measure survival fractions as low as 1 x 10^{-4}.

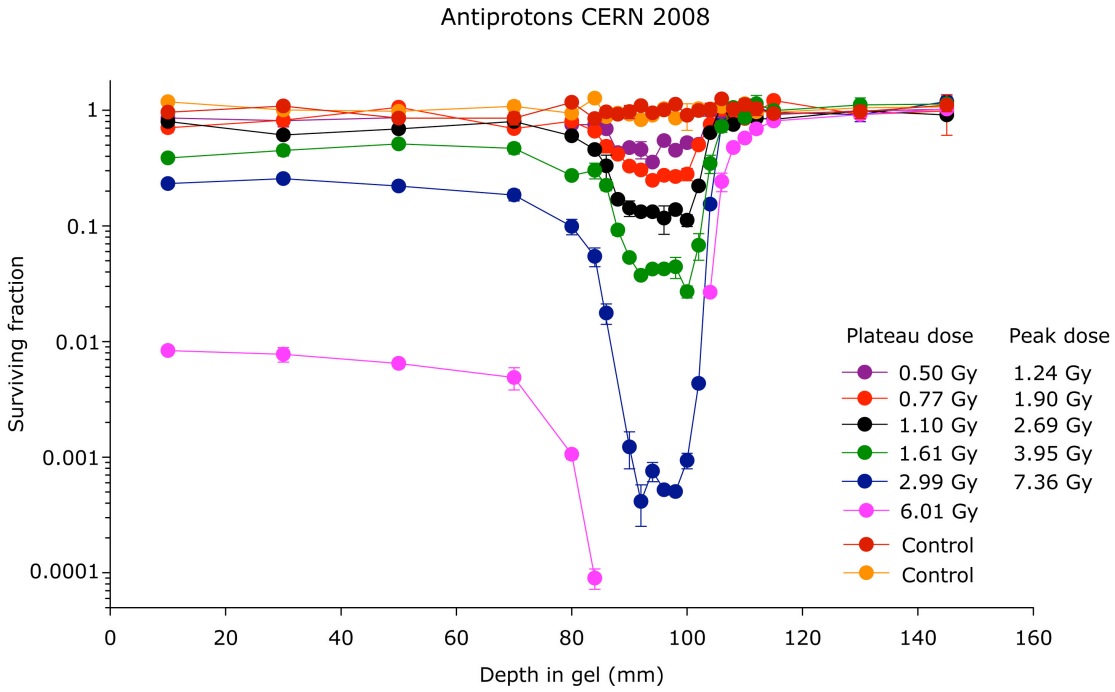

Fig. 1: Survival fraction vs. depth in the target for V79 Chinese Hamster cells irradiated with antiprotons during the 2008 run period.

In 2009 we continued these measurements with a focus on obtaining statistically significant data distal to the Bragg peak. After taking a few low dose runs to establish the exact position of the survival curve we then took long irradiation periods to achieve plateau doses of nominally 18 and 23.5 Gy. But even at these high dose levels the survival returned to values of 50% and higher 2 mm past the distal edge of the Bragg peak (100 mm). The slice at 102 mm is the only one yielding a large enough data spread to achieve a realistic fit of the linear-quadratic dose response curve to the data. From this one fit we conclude that the RBE is already returning towards the plateau value.

Our aim fo the 2010 run was to add a second data et to the 2009 data for statistical accuracy. Despinte the fact that we lost nearly 24 hours of beam, due to the ad-hoc machine development time in the middle of the week and the problem in starting up the AD again after the MD, we were able to collect survival data for 9 dose points between 0.5 and 5 Gy.

Figure 2 shows the raw survival data plotted versus the penetration depth into the target. This initial plot does not yet include error bars and must be considered preliminary.

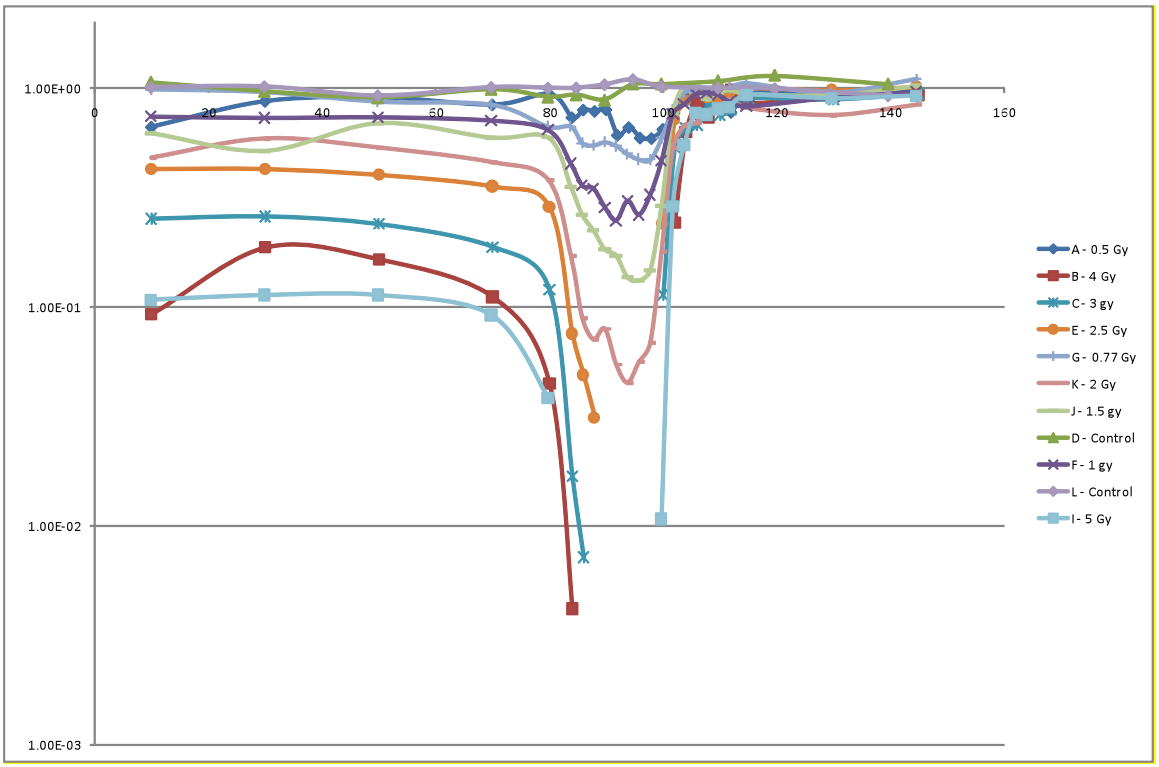

Fig. 2: Survival fraction vs. depth in the target for V79 Chinese Hamster cells irradiated with antiprotons during the 2010 run period.

We now can use the data sets from 2007, 2008, 2009 and 2010 to analyse the dose response in the plateau region. Following the observation that the response stays essentially flat up to the proximal edge of the spread out Bragg peak we group the survival values for 10, 30, 50, and 70 mm together for each dose value and plot these vs. dose. Figure 3 shows the survival data from the 2010 run period

together with a combined fit to all data from 2007, 2008, and 2009. This supports the value for the $RBE_{plateau}$ = 1.25 reported last year. A final result will be obtained when all runs are completed and the data set is significant larger. Also, after several repeat experiments we will be able to include error bars in order to improve the fit quality.

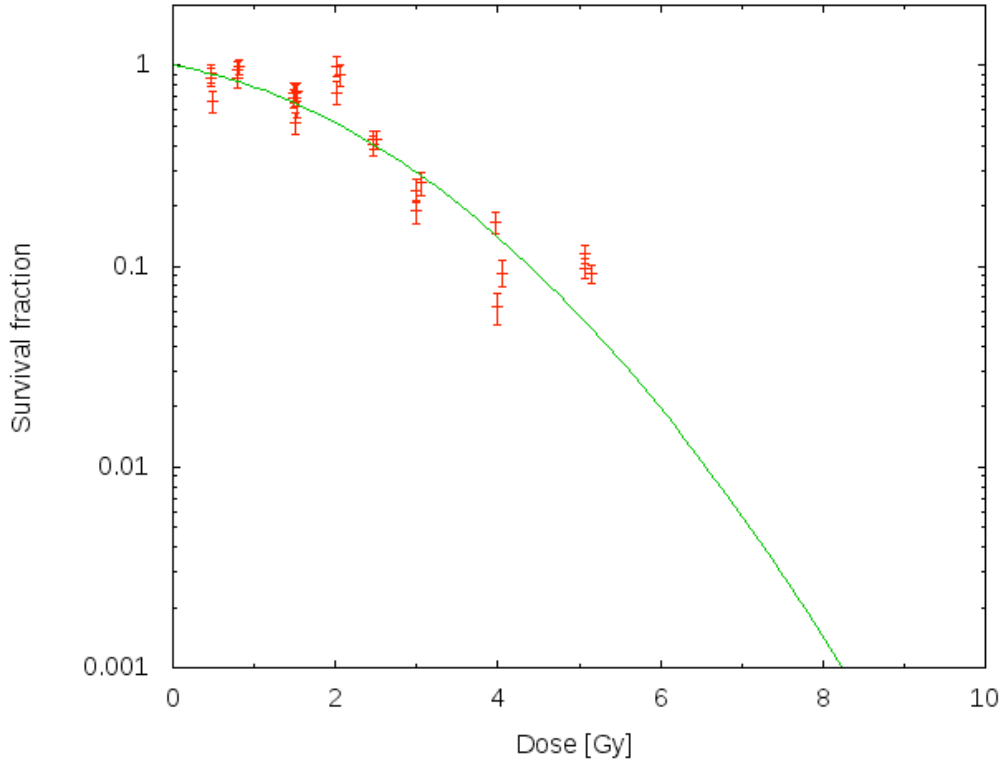

Fig. 3: Survival fraction vs. dose in the plateau region for V79 Chinese Hamster cells irradiated with antiprotons. The red points are the data obtained during the 2010 run time, the green line is the result of a fit to all data points obtained during the three previous years.

The error bars in figure 3 and 4 include only the standard deviation from three platings obtained in a single dose point. Errors are not purely statistical but are due to variations in cell preparation, plating, and in response to this it is established practice in radiotherapy experiments to repeat experiments several times and then use the standard deviation of the entire sample as error bar. To do this we need to assure that we get survival data in independent experiments at the same dose point. For the plateau region this is relatively easy as small shifts in dose value can be corrected since the RBE in the plateau is constant, and we are currently in the process to construct a meta-analysis to establish the overall error bars both in survival and in dose for the entire data set.

This analysis is a much more difficult task in the peak region, where we superimpose Bragg peaks with different ranges, so that at each depth point a given dose value can consist of different mixtures of RBE values and therefore yield a different survival value for the same depth and dose point, dependent on the detailed set-up of the experiment. To achieve this we needed to have a much more stringent control on beam intensity and position fluctuations in order to produce identical situations in independent experiments. This was the primary reason for us to develop a new beam monitoring system to allow shot to shot analysis of shape, intensity, and position of each extracted AD pulse (see Appendix II).

Until this task has been completed we cannot combine data from 2010 with the data from prior years to extract a value for the relative biological efficiency for the distal edge of the spread out Bragg peak and points in the transition region from plateau to peak, which is of highest importance for quantitative comparitive dose planning studies. We aim in adding two independent sets of measurements to the existing data set in 2011 to achieve sufficient statistical accuracy for this.

Figure 4 displays the survival data obtained for cells located at the distal edge of the spread-out Bragg peak, and initial inspection shows, that these values agree well with the measurements from prior years.

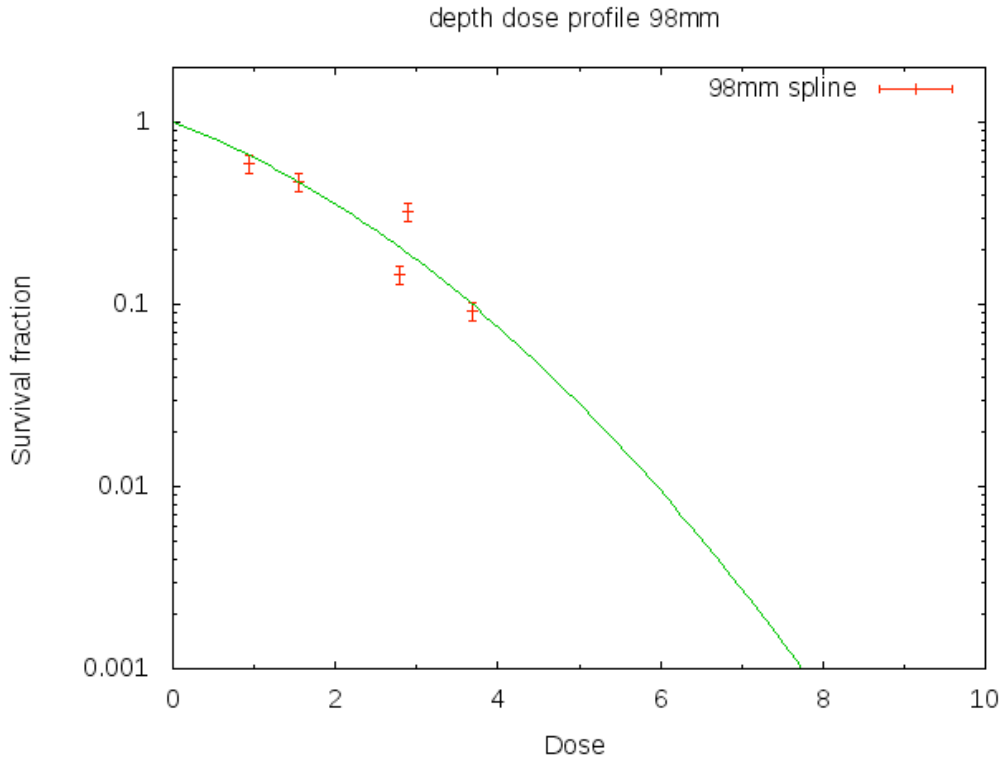

Fig. 4: Survival fraction vs. dose for the distal edge of the spread-out Bragg for V79 Chinese Hamster cells irradiated with antiprotons.

III. **Shot-by-shot monitoring of the antiproton beam.**

As mentioned before, the knowledge of the exact profile and position of the beam during sample irradiation is of utmost important to the qulaity of the results. Cell survival depends exponentially on the dose delivered and with the typical beam size at the DEM line of approximately 7 mm FWHM, the variation in dose across the 6 mm active tube diameter is significant. Initially this effect was mitigated by using a much broader beam spot which unfortunately significantly reduces the dose rate to the target and increases the irradiation time to the samples to the point where 1 week of beam time would not suffice for a complete data set.

With better beam monitoring and advances in our Monte Carlo dose calculations it became possible to account for the inhomogeneity by more precise calculations of the 3-dimensional dose distribution. The remaining disadvantage was then that the profile measurement took a minimum of 20 to 30 individual beam shots and only provided the average distribution over the entire sample. The highly non-linear response of the cells would then not allow to account properly for short term variations of position and shape of the beam.

In search for a shot-by-shot measurement of the beam parameters we came across the developmental project of the Mimotera (Minimum Ionizing MOnolithic active pixel detector for the TERA foundation). We invited Prof. Caccia from the University of Insurbia, Como, Italy to join the AD-4 collaboration and assigned a diploma student from the MPI-K, Heidelberg, Germany as the lead person to the adaptation and commissioning of the Mimotera for the ACE experiment. This collaboration resulted in a detector system capable of detecting and displaying online an image of each antiproton pulse delivered to the front end of our experiment. Figure 5 shows a representative example of the resulting online display.

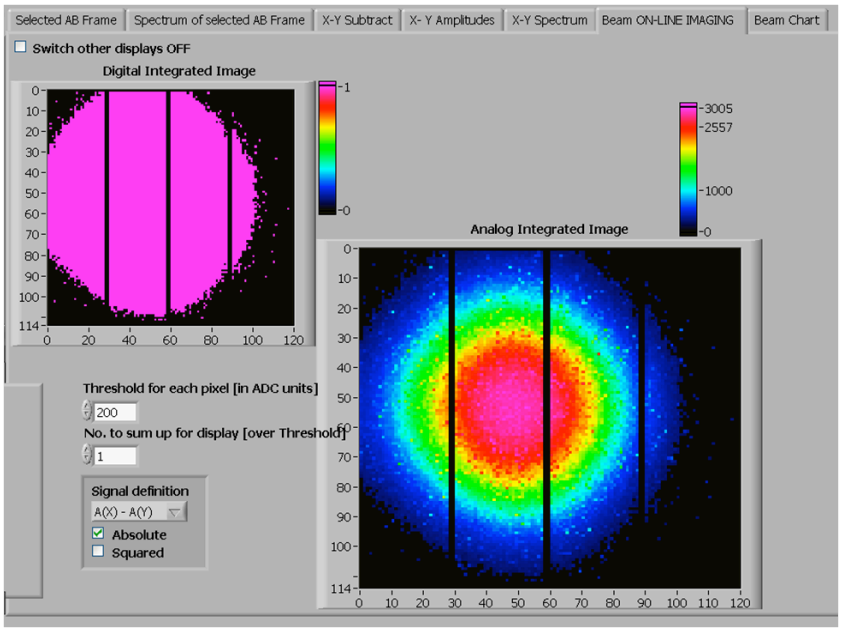

Fig. 5: Online image of the beam profile of a single antiproton shot from the AD. The dark vertical stripes are electronic markers only, to be used by the data acquisition system. The pixel size is 150 x 150 µm, which allows alignment of the beam to a sub-millimeter precision.

Not only does this allow a shot-by-shot dose analysis for irradiated samples, but it also provides an immediate detection of any beam changes that could affect the quality of an individual experiment. Figure 6 shows an example for such an event: in the middle of a long irradiation it was suddenly noticed that the beam was changing back and forth between a circular and an elliptical profile, latter exposing the sample to a much higher dose in the central region than the nominal value. Irradiation was immediately stopped and the sample removed from the target station. Observing the beam profile for a few more shots then suddenly revealed a shift of several millimeters to the right. An AD operator was called to the control room (the event happened on Saturday) and after his arrival and a reset of one of the quadrupole magnets it took him about 5 shots to get the beam back to the nominal parameters. Under previous conditions this would have been gone unnoticed and would have rendered the measurement unusable, or, even worse, would have added a wrong data point to our set without us having an indication of the error.

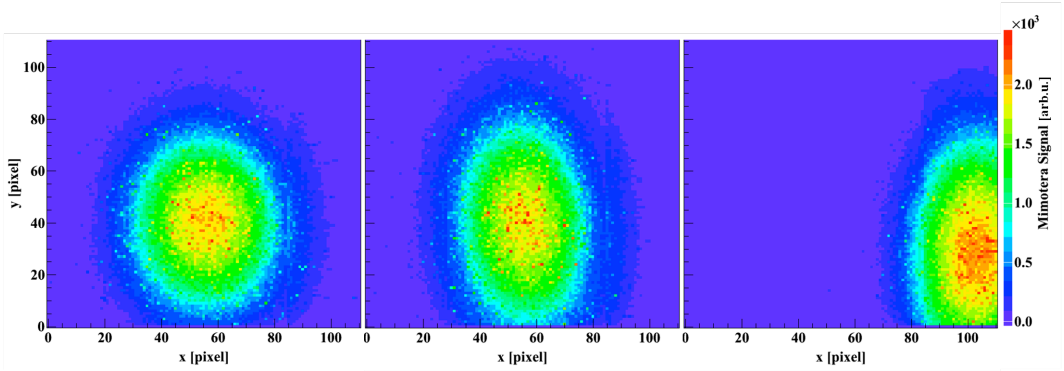

Fig. 6: Beam images obtained at the AD during the 2010 run period. Initially the beam started oscillating between a near circular shape (left frame) and a vertical ellipse (middle frame). After a short while the beam suddenly shifted drastically to the right. It was found that one coil in a quadrupole magnet had failed and a quick repair brought the beam back to it's nominal shape, allowing continuing with the long time irradiation planned for this time period.

A second Mimotera chip has been installed at the far end of the ACE experiment and the combination of the two detectors can now be used to quickly align the experimental set-up to the true beam position.

A paper accepted for publication in Radiation Measurement is attached as Appendix I. Technical details are contained in the Diploma Thesis of Rebecca Boll, Max Planck Institute for Nuclear Physics, Heidelberg, Germany.

IV. **Real-time imaging of the antiproton annihilation in biological targets.**

The main physical advantage of charged particle cancer therapy is to be found in the inverse dose deposition profile (the Bragg Peak), which allows to deposit energy to a volume at a prescribed depth in the human body by varying the energy of the incoming particle. This leads to significant sparing of normal tissue and is believed to lower side- and late effects and allows to increase the dose to the tumour with the goal to achieve better tumour control. On the other side, having such a precise tool can also easily lead to errors. The penetration depth of a charged particle in the target strongly depends on the exact density profile along its path and cannot always be calculated with the desired precision due to unknow density variations in space ant time and difficulties of converting densities of CT Images obtained prior to the treatment to density numbers.

The holy grail in particle therapy therefore is the direct detection of the dose deposition during the treatment. Efforts in this direction consist of PET imaging of beta-emitting isotopes generated during the treatment by nuclear reactions with the target atoms. PET imaging for carbon ion therapy has been developed at GSI and has been successfully used on many patients. But the time delay between irradiation and diagnostics due to the life time of the beta-emitters and the time needed to generate sufficient signal-to-noise for good quality images has allowed it to be used only as an interfractional tool, detecting an error in oe radiation session before the next session commences, typically on the next day.

Photons generated by interactions between projectile ions and target atoms also produce high energy gammas, and detecting these with the so-called prompt gamma camera is an active field of research.

Antiprotons offer a distinct advantage in this respect, as the annihilation event at the end of the flight path generates several prompt high energy charged pions as well as high energy gammas from the prompt decay of neutral pions. These can be detected with external instruments and tracing their flight path back allows vertex reconstruction for single annihilation events. This method has been used by many high energy experiments and also by the ATHENA collaboration during the early years of antihydrogen production in Penning traps.

Our goal consisted of demonstrating the feasibility of real time imaging of the distal edge of an antiproton beam stopping in a biological phantom at a reasonable cost. For this purpose we teamed up with the team of Petra Riedler, who provided us with a ladder of 10 chips used in the ALICE inner tracker. In order to obtain tracking information with just one layer of silicon detectors we mounted the ladder in such a way that the detector was pointing with his thin edge towards the annihilation region, and actually a few degrees beyond, to avoid ambiguities from tracks originating from points in front and in back of the Bragg peak. Figure 7 gives a schematic view of the set-up.

Due to limitations in the occupancy rate of the detector read-out together with the extreme momentary event rate of approximately 6×10^{13} annihilations/second during the 500 ns long beam pulse, the detector had to be placed about 1.4 meter away from the target. This severely limited the resolution in determining the stopping distance along the beam axis (figure 8). For the hypothetical case of a continuous beam of antiprotons with the same integrated intensity the resolution of the same set-up was modeled by Monte Carlo calculations to be in the order of a few millimeter (see figure 9).

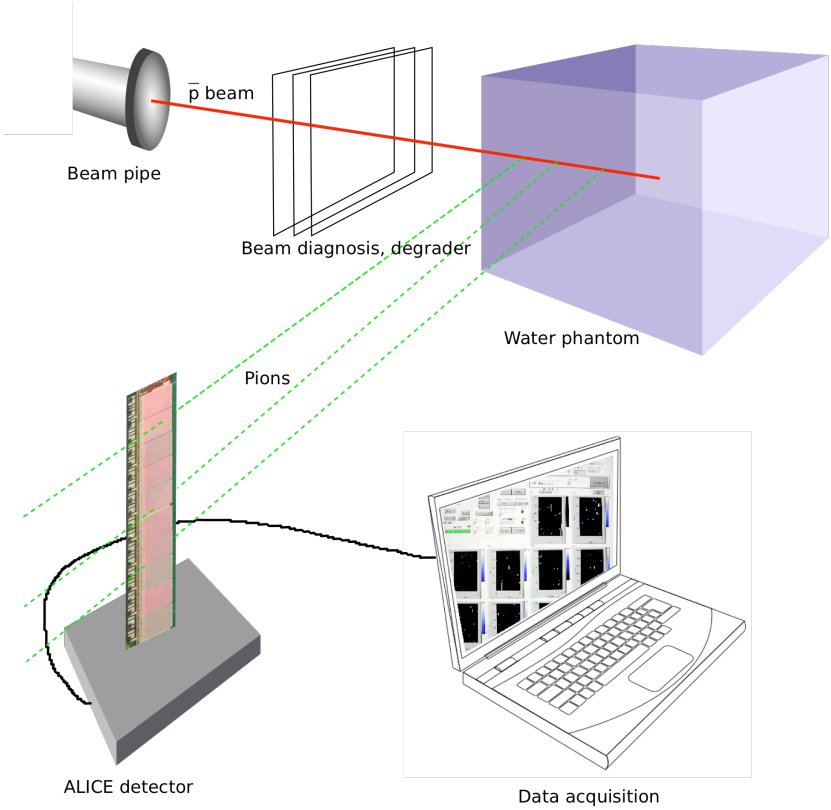

Fig. 7: Schematic of set-up for real time imaging of antiproton annihilation. The narrow edge of the detector points slightly beyond the Bragg Peak. Pions originating from an area proximal of the Bragg peak will leave short tracks in the detector. When the annihilation points move closer to the Bragg peak these tracks will get longer and longer. Using the track length information alone, a position in z-direction can be deduced.

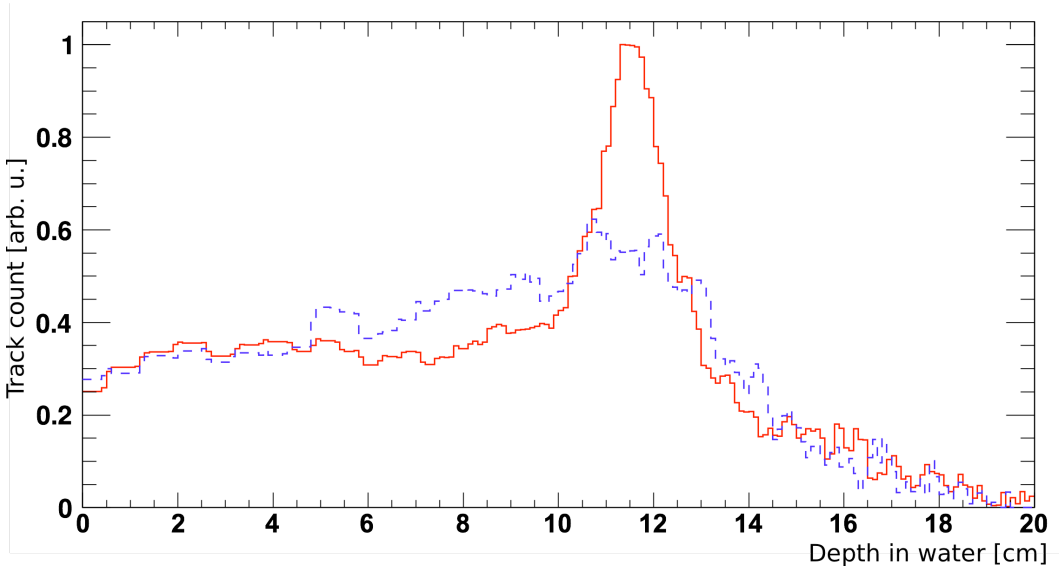

Fig. 8: Histogram of track length distribution. The difference between simulation (red) and experimental data (blue) is due to the multiple scattering of the pions when leaving the water tank. In particular the measured annihilation vertex distribution is very broad. This is due to multiple scattering of the pions within the water phantom, which is magnified by the large distance between phantom and detector. As a consequence, the distribution is blurred by a Gaussian distribution with a FWHM of about 9 cm, leading to a long tail behind the distal end of the Bragg peak.

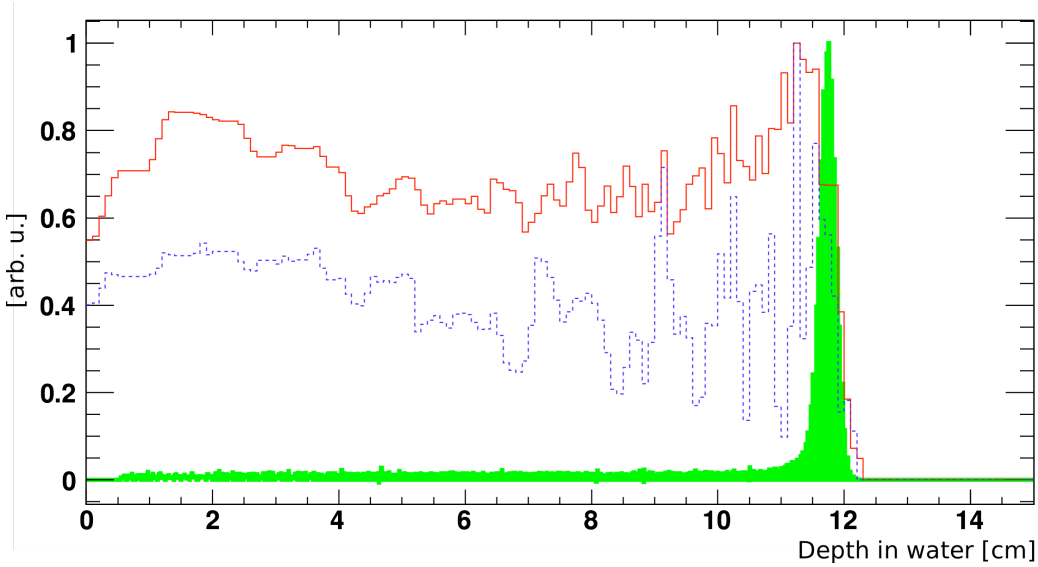

Fig. 9: For the more clinical example, 50 times 40 million antiprotons were simulated with the distance between the detector and the water phantom decreased to 30 cm. Here, the maximum of the differential antiproton fluence (green) coincides perfectly with the shoulder of the reconstructed annihilation vertex distribution (red). The range of the antiprotons can be determined in the order of a few millimeters after the very first fraction of the irradiation as shown by the blue line, where the signal of only 10^8 antiprotons was evaluated.

This preliminary work proofs the feasibility of detecting the location of antiproton annihilations for a small number of particles compared to the number needed to administer one clinical fraction of the therapy. This opens up the possibility to follow the irradiation progress in real time and correct for eventual deviations during the treatment itself.

A short report of this work, to be published in Radiation Measurements is contained in Appendix II. More details can be found in the Diploma Thesis of Stefan Sellner, Max Planck Institute for Nuclear Physics, Heidelberg, Germany.

V. Other Activities

DNA damage and repair studies.

The team from the Quen'sUniversity in Belfast used some of the breaks between cell survival measurements to continue their work from last year.

Due to the experimental sessions occurring late in the year and the long post irradiation processing times, this report is mainly based on the 2009 data with samples from the 2010 experiments still being processed. Our initial plans for the AD4 beam time in October of 2010 were to:

- Extend our DNA damage studies to 24 hrs post irradiation in order to further investigate the different quality of DNA lesions produced in the plateau and SOBP and how cells respond to them.
- Repeat and extend the micronuclei experiments to validate previous results and widen the sub-lethal investigations to out of beam samples (i.e. secondary particle and bystander effect).
- Investigate possible use of plasmids as a fast (<2 hours) biodosimeter

As a result of a significant loss of beam time, more than one half of the planned experiments could not be carried out. In order to complement our previous experiments and to make the best use of the available time we irradiated human fibroblast cells in plateau, centre of the SOBP and outside the beam with plateau doses from 0-2 Gy. By culturing the cells for 24hrs post irradiation, the repair of DNA damage in these cells was then analyzed to investigate how the different complexity of damage (described earlier in this text) affect the cell's outcome.

Data analysis from these experiments is ongoing and will be available in 2011.

A full report on the continuation of studies of irradiated cells on the DNA level is contained in Appendix III.

Liquid Ionization Chambers for RBE Determination

The continuation of the studies to use liquid ionization chambers to extract RBE information from the response was hindered by several problems with the beam during LIC measurement periods. The most significant problem was the constantly changing cycle time, due to demands form other users on the PS, which caused a mis-match with the trigger number and difficulties in identifying which monitor chamber reading corresponds to which LIC reading.

Off line we have made significant progress in developing methods and protocols for extracting RBE, using beams of electrons and ions. Several papers on this work were published and will be applicable to antiproton measurements in the next run, hopefully with a more stable operations scheme.

To best exploit the techniques developed during the last years at CERN it would be advantageous to run with two different dose rates. This could for instance be achieved by change the focus. This was not tried before for fear that resetting the beam to its original conditions, but should be easy to do now with the new beam monitor in place.

VI. Summary, Outlook, and Beam Time Request

Using a total of less than seven weeks of beam time over the last 7 years (equivalent to approximately 4 hours of beam time at a clinical installation like the Heidelberg Heavy Ion Therapy Center) we have now reached the point where we have developed reliable tools for physical dosimetry and beam delivery planning. This has allowed us to collect over the last 3 years an initial data set on the relative biological efficiency (RBE) of antiprotons for the chosen endpoint of 10% clonogenic survival of V-79 Chinese Hamster cells. We observe a steep increase of RBE for antiprotons at the proximal edge of a spread-out Bragg peak (SOBP), in contrast to carbon ions, where RBE is increasing gradually along the beam path.

Biological measurements are burdened by large uncertainties and to quantify these findings and apply them to comparable treatment planning exercises on specific tumor incidents that are believed to be prime candidates for a future antiproton therapy application, we have to perform a number of independent repeat experiments in order to confirm our current data and achieve a high statistical significance. Individual data sets are sparse and we need to accumulate more data points for each depth slice in the target in order to obtain higher quality fits. Only then we can expand the initial dose planning studies shown in last year's report by including the actual variation of RBE with depth for both carbon ions and antiprotons.

In addition to RBE in the target area for clonogenic survival an equally, if not more important, question we have started to address is the effect of DNA damage and genetic mutation, and the relation to possible tumorigenesis. Such late effects are an active topic of discussions in all radiotherapy modalities, and we expect more physical and biological studies in this field to become available in the next years to which we can compare our results.

As a support of the biological studies we have developed dosimetric tools for mixed radiation fields and have benchmarked our preferred Monte Carlo code (FLUKA) against experimental data. We have shown the possibilities for absolute dosimetry using Alanine pellets and have continued our development of linear energy transfer (LET) measurements using liquid ionization chambers. To improve our data taking capability at the AD we have developed novel beam monitors and have significantly upgraded our experimental set-up in order to accommodate the development of the new AEGIS experiment sharing the same beam line.

Proof-of-principle of real time imaging of the annihilation distribution have been performed and have demonstrated that the Bragg peak position can be detected with a simplified set-up. Momte Carlo studies based on the measurements at CERN in 2009 and 2010 predict millimeter-precision in the detection of the distal edge of an incoming beam delivering the same amount of antiprotons in a continuous fashion, lowering the instantaneous rate and allowing setting the detector closer to the patient.

With the limited data set we have been able to accumulate in the few weeks of beam time since inception we have now reached a point where many of the initial questions have been addressed and a potential of a future use of antiprotons in cancer therapy can be argued. We now need to improve the statistical quality of the data set to apply our knowledge to comparative dose planning exercises on specific, clinical relevant, tumor incidents.

To allow us to move forward in this research efficiently we request a slight expansion of the current procedure, where two weeks of AD beam time at 500 MeV/c is dedicated to our experiment. This would enable us to accumulate two additional independent data sets for the clonogenic survival, hopefully completing this study. Unavoidable down time during the clonogenic survival measurements, given by the logistics of transporting cells to and from CERN would be used for a continuation and enhancement of DNA damage studies, and the development of LET measurements with Liquid Ionization Chambers (LIC). Considering the 26 weeks of AD Physics time typically available in a given year, this is less than 10% of the total beam available. To set the amount of beam time in perspective: the overall number of antiprotons delivered to AD-4 since inception is equivalent to just a few hours of beam time at a carbon ion therapy facility.

Compared to 2010, where we were granted an additional 7 shifts for detector development, this request represents an increase of 14 shifts.

We request that the two weeks are separated by several months, allowing the analysis of the first run period to be completed before the second run. The second run could be scheduled for the last week of the AD run schedule.

VI. Acknowledgements

This work would not have been possible with out the support of the AD operation team. They have shown extreme motivation in providing the beam conditions needed for these measurements and have worked creatively in providing solutions to our needs without causing major interference with the main program of ultra-low energy antiproton physics of the AD community. We appreciate the help, support, and continued interest of many of our colleagues at the AD and many members of the CERN administrative, technical, and scientific staff.

The work was financially supported through many funding agency around the world, supporting the different institutions involved, as well as by special grants from the Danish Cancer Foundation and the European Union Marie-Curie Fellowship program.

Updated List of publications from the AD-4 Collaboration

1. Bassler, N., Holzscheiter, M.H., Petersen, J.B., 'Neutron Fluence in Antiproton Radiotherapy, Measurements and Simulations', *submitted to Acta Oncologica*
2. Bassler, N., Kantemiris, I., Karaiskos, P., Engelke, J., Holzscheiter, M.H., Petersen, J.B. 2010; Comparison of optimized single and multifield irradiation plans of antiproton, proton, and ion beams, *Radiotherapy & Oncology (2010) vol. 95, pp. 87 – 93*
3. Kantemiris, I., Angelopoulos, A., Bassler, N., Giokaris, N., Holzscheiter, M., Karaiskos, P., Kalogeropoulos, T.E., 'Real-time imaging during antiproton radiotherapy', *Phys. Med. Biol. (2010) vol. 55, pp. N1–N9*
4. Fahimian, B.P., DeMarco, J.J., Keyes, R., Bassler, N., Iwamoto, K.S., Zankl, M., Holzscheiter, M.H., 'Antiproton radiotherapy: peripheral dose from secondary neutrons', *Hyperfine Interact (2009) vol. 194, pp. 313–318*
5. J.N. Kavanagh, F.J. Currell, D.J. Timson, M.H. Holzscheiter, N. Bassler, R. Herrmann, G. Schettino; 'Induction of DNA Damage by Antiprotons for a Novel Radiotherapy Approach'; *submitted to European Physical Journal D* (2009)
6. Niels Bassler, Ioannis Kantemiris, Julia Engelke, Michael Holzscheiter, Jørgen B. Petersen, 'Comparison of Optimized Single and Multifield Irradiation Plans of Antiproton, Proton and Carbon Ion Beams', submitted to *Radiotherapy and Oncology* (2009)
7. Bassler, N., Holzscheiter, M.H., Petersen, J.B., 'Neutron Fluence in Antiproton Radiotherapy, Measurements and Simulations', submitted to *Physics in Medicine and Biology* (2009)
8. Kantemiris, I., Angelopoulos, A., Bassler, N., Giokaris, N., Holzscheiter, M., Karaiskos, P., Kalogeropoulos, T.E., 'Real-time imaging for dose evaluation during antiproton irradiation', *Physics in Medicine and Biology*, in print (2009)
9. Kovacevic, S., Bassler, N., Hartley, O., Vranjes, S., Garaj-Vrhovac, V., Holzscheiter, M., 'V-79 Chinese Hamster Cells irradiated with antiprotons, a study of peripheral damage due to medium and long range components of the annihilation radiation', *Int. J. of Rad. Biology* 85: pp. 1148-1156 (2009)
10. Fahimian, B.P., DeMarco, J.J., Keyes, R., Bassler, N., Iwamoto, K.S., Zankl, M., Holzscheiter, M.H., 'Antiproton radiotherapy: peripheral dose from secondary neutrons', *Hyperfine Interaction* 194: pp. 313-318 (2009)
11. Bassler, N., Holzscheiter, M. 2009, 'Calculated LET Spectrum from Antiproton Beams Stopping in Water', *Acta Oncologica* 48: pp. 223-226 (2009)

12. Niels Bassler, Jan Alsner, Gerd Beyer, John J. DeMarco, Michael Doser, Dragan Hajdukovic, Oliver Hartley, Keisuke S. Iwamoto, Oliver Jäkel, Helge V. Knudsen, Sandra Kovacevic, Søren Pape Møller, Jens Overgaard, Jørgen B. Petersen, Timothy D. Solberg, Brita S. Sørensen, Sanja Vranjes, Bradly G. Wouters, Michael H. Holzscheiter; 'Antiproton radiotherapy', *Radiotherapy and Oncology* 86: pp. 14-19 (2008)

13. Knudsen, H., Holzscheiter, M.H., Bassler, N., Alsner, J., Beyer, G., DeMarco, J.J., Doser, M., Hajdukovic, D., Hartley, O., Iwamoto, K.S., Jäkel, O., Kovacevic, S., Møller, S.P., Overgaard, J., Petersen, J.B.B., Ratib, O., Solberg, T.D., Vranjes, S., Wouters, B.G., the CERN ACE Collaboration, , 'Antiproton Therapy', *Nuclear Instruments and Methods in Physics Research B* 266: pp. 530-534 (2008)

14. Bassler, N., Holzscheiter, M., Jäkel, O., Knudsen, H., Kovacevic, S., AD-4/ACE Collaboration, 'The Antiproton Depth-Dose Curve in Water', *Physics in Medicine and Biology* 53: pp. 793-805 (2008)

15. Bassler, N., Hansen, J.W., Palmans, H., Holzscheiter, M.H., Kovacevic, S., 'The Antiproton Depth Dose Curve Measured with Alanine Detectors', *Nuclear Instruments and Methods in Physics Reseach B* 266: pp. 929-936 (2008)

16. Bassler, N., Knudsen, H., Møller, S.P., Petersen, J.B.B., Rahbek, D., Uggerhøj, U.I., 'Bubble detector measurements of a mixed radiation field from antiproton annihilation', *Nuclear Instruments and Methods in Physics Research B* 251: pp. 269-273 (2006)

17. Holzscheiter, M.H., Bassler, N., Agazaryan, N., Beyer, G., Blackmore, E., DeMarco, J.J., Doser, M., Durand, R.E., Hartley, O., Iwamoto, K.S., Knudsen, H., Landua, R., Maggiore, C., McBride, W.H., Møller, S.P., Petersen, J.B.B., Skarsgard, L.D., Smathers, J.B., Solberg, T.D., Uggerhøj, U.I., Vranjes, S., Withers, H.R., Wong, M., Wouters, B.G. 2006, 'The biological effectiveness of antiproton irradiation', *Radiotherapy & Oncology* 81: pp. 233-242 (2006)

18. Bassler, N., Holzscheiter, M.H., Knudsen, H., 'Cancer therapy with antiprotons', in *Low Energy Antiproton Physics-LEAP '05, AIP Conference Proceedings CP769*, pp. 423-430 (2005)

19. Holzscheiter, M.H., Agazaryan, N., Bassler, N., Beyer, G., DeMarco, J.J., Doser, M., Ichioka, T., Iwamoto, K.S., Knudsen, H., Landua, R., Maggiore, C., McBride, W.H., Møller, S.P., Petersen, J.B.B., Skarsgard, L.D., Smathers, J.B., Solberg, T.D., Uggerhøj, U.I., Withers, H.R., Vranjes, S., Wong, M., Wouters, B.G. 2004, 'Biological effectiveness of antiproton annihilation', *Nuclear Instruments and Methods in Physics Reseach B* 221: pp. 210-214 (2004)

20. Maggiore, C., Agazaryan, N., Bassler, N., Blackmore, E., Beyer, G., DeMarco, J.J., Doser, M., Gruhn, C.R., Holzscheiter, M.H., Ichioka, T., Iwamoto, K.S., Knudsen, H., Landua, R., McBride, W.H., Møller, S.P., Petersen, J.B.B., Smathers, J.B., Skarsgard, L.D., Solberg, T.D., Uggerhøj, U.I., Withers, H.R., Wouters, B.G., 'Biological Effectiveness of Antiproton Annihilation', *Nuclear Instruments and Methods in Physics Research B* 214: pp. 181-185 (2004)

Appendix I

Using Monolithic Active Pixel Sensors for Fast Monitoring of Therapeutic Hadron Beams

R. Boll[a], C.P. Welsch[b], M.H. Holzscheiter[a,c]

[a]Max-Planck-Institute for Nuclear Physics, Heidelberg, Germany.
[b]Cockcroft Institute and University of Liverpool, UK.
[c]University of New Mexico, Albuquerque NM, USA.

Available online at www.sciencedirect.com
ScienceDirect
Radiation Measurement 00 (2010) 1–4
Radiation Measurement

Using Monolithic Active Pixel Sensors for Fast Monitoring of Therapeutic Hadron Beams

R. Boll[a], C.P. Welsch[b], M.H. Holzscheiter[a,c]

[a] *Max-Planck-Institute for Nuclear Physics, Heidelberg, Germany.*
[b] *Cockcroft Institute and University of Liverpool, UK.*
[c] *University of New Mexico, Albuquerque NM, USA.*

Abstract

It has been shown that Monolithic Active Pixel Sensors (MAPS) are very promising tools for direct online beam monitoring, for current heavy ion therapy facilities as well as for future innovative cancer treatments with antiprotons. More specific, the dead-time free *Mimotera* sensor has been proven to be capable of dealing with extremly short pulses of antiprotons of only 500 ns duration, as well as with continuous beams of carbon ions in the complete intensity- and energy range used in today's heavy ion facilities. It shows a linear behavior up to 7.5×10^7 antiprotons per square centimeter in 500 ns and up to 8×10^8 carbon ions per square centimeter per second .

Keywords:
Monolithic Active Pixel Sensor, Mimotera, Beam monitor, Cancer therapy, Antiprotons

1. Introduction and Motivation

Nowadays, tumors are most frequently treated by irradiation with X-rays. Anyhow, in the last 60 years a new technology has been developed that is especially beneficial for deep seated tumors and and which is in clinical use since 1990 [1]: The treatment of cancer with hadron beams, most commonly with protons or carbon ions. From a biological point of view, heavy ions have one outstanding advantage over photons, namely the mechanism of energy loss along their path through the body, resulting in a sharp rise of the energy deposition at the very end of their track, called the Bragg-peak. The idea of using antiprotons for cancer therapy, however, is rather new [2] and there is only one experiment worldwide doing research on this: The Antiproton Cell Experiment (ACE) [3], located at the Antiproton-Decelerator (AD) of the European Organization for Nuclear Reseach (CERN).

The physical behavior of antiprotons is very similar to protons, with one crucial difference: Once the antiproton annihilates with a proton at the end of its range, it releases an additional energy of $2 \times 936\,\mathrm{MeV} = 1.87\,\mathrm{GeV}$ per particle as compared to protons, of which a small but clinically significant fraction is deposited locally. This means that to achieve the same energy transfer to the tumor in the Bragg-peak region, half as many particles are needed and the dose in the entrance channel in front of the tumor is reduced, sparing healthy tissue and organs at risk.

The experimental set-up at ACE is as follows: The antiproton beam enters a Poly(methyl methacrylate)(PMMA)-tank which contains a probe of V-79 Chinese Hamster cells embedded into gelatin. For reasons of cooling it is surrounded by a mixture of water and glycol, that also simulates the back scattering from a real biological target. After the irradiation, cell survival curves are obtained from evaluating the probes. As the biological effect of particles on living cells is the quantity to be evaluated, it is crucial to know as precisely as possible the physical characteristics of the incident beam as the input parameters for all following analyses. The properties necessary for the evaluation

of the data are the diameter and the shape of the beam profile, the fluctuations of the beam intensity from shot to shot and the beam position.

The situation at ACE is unique in the sense of the spill structure: The beam of antiprotons is pulsed, one spill is 500 ns long and arrives only every 90 s due to the accelerator architecture. During these 500 ns, the intensity is about 3×10^7 particles, which leads to a momentarily integrated intensity of $3 \times 10^7/(500\,\text{ns} \times 0.4\,\text{cm}^2 \times \pi) = 1.19 \times 10^{14}\text{s}^{-1}\text{cm}^{-2}$. The beam energy is 126 MeV.

For this special situation a detector is required that is capable of handling this amount of particles in such a short time. It must not saturate in order to be able to get the true number of particles for each pixel and it must provide a fast, digital output for every single shot, which can then immediately be used for correcting the beam, if necessary. Previous systems such as ionization chambers, gafchromic films or scintillating screens were lacking at least one of these abilities. This gave rise to the search for a new device, the most promising candidate being a Monolithic Active Pixel Sensor (MAPS).

2. Architecture of the sensor

The *Mimotera* (**M**inimum **I**onizing **MO**nolithic active pixel detector for the **TERA** foundation) is a MAPS of crystalline silicon. The epitaxial layer is only 14 μm thick and has an entrance window of only about 100 nm. [4] This is possible by thinning the wafer down and back-illuminating it. The sensor consists of $112 \times 112 = 12544$ pixels, each of the size of $153 \times 153\,\mu\text{m}^2$. This leads to an active area of $17 \times 17\,\text{mm}^2$, which is divided into four sub-arrays of 28×112 pixels that are read out in parallel with a frame rate up to 10 kHz. Moreover, there are two rows and two columns per sub-quarter which act as so called "dummy-pixels". These are not physical pixels, so there is no dead area on the sensor, but they are introduced to allow matching the one-dimensional, linear analog output with the two-dimensional matrix in the data analysis. The maximum readout rate for one single pixel is 20 MHz, which corresponds to $1/20\,\text{MHz} = 50\,\text{ns}$. The readout of one sub-array therefore takes $50\,\text{ns} \times (112+2) \times (28+2) = 170\,\mu\text{s}$. As the four sub-arrays are read out in parallel, this is identical to the readout time for one frame of the whole detector. In the following measurements a clock rate of 2.5 MHz per pixel has been chosen, which leads to an integration time of 1.4 ms.

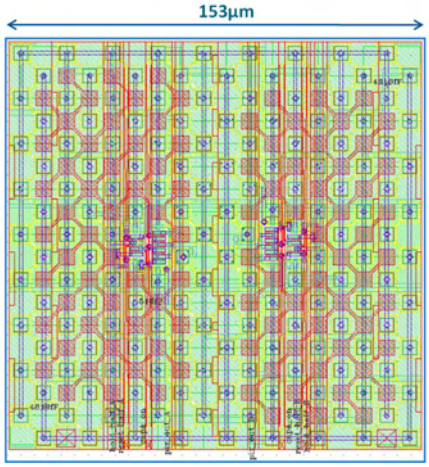

Figure 1: Design of one of the pixels of the *Mimotera*. All red and all yellow diodes are connected, building two completely independent, interleaved readout matrices for each of the pixels. *(Courtesy of M. Caccia)*

The design of one single pixel makes the *Mimotera* a unique device: Each of the pixels consists of 2×81 diodes, $5 \times 5\,\mu\text{m}^2$ each, corresponding to the red and yellow squares in Figure 1, building two independent readout matrices which will in the following be referred to as matrix A and matrix B. This architecture makes the *Mimotera* a detector without any dead time: While matrix A is collecting the generated charge carriers, the charges stored in the diodes of

matrix B are read out, the diodes are reset, afterwards the process is inverted. Hence, no signal charges get lost during the readout and the detector is free of dead time.

3. Measurements at CERN

In June 2010 first tests have been carried out at ACE. The beam spill of 500 ns duration is contained in only one readout frame of 1.4 ms of the sensor. Therefore it is most convenient to analyze the data in a differential way, subtracting the frame with the spill from the previous one without beam. This has the advantage that one does not have to record pedestal files. All dead pixels and time-dependent background signals are eliminated automatically.

The crucial question for the first test run was to find out whether the detector is really capable of coping with the high momentary intensity of ACE. Investigations into possible saturation effects in the beam core were carried out. If such effects were present, they would limit the detector's capability of measuring the full beam intensity and determining the beam profile with high precision.

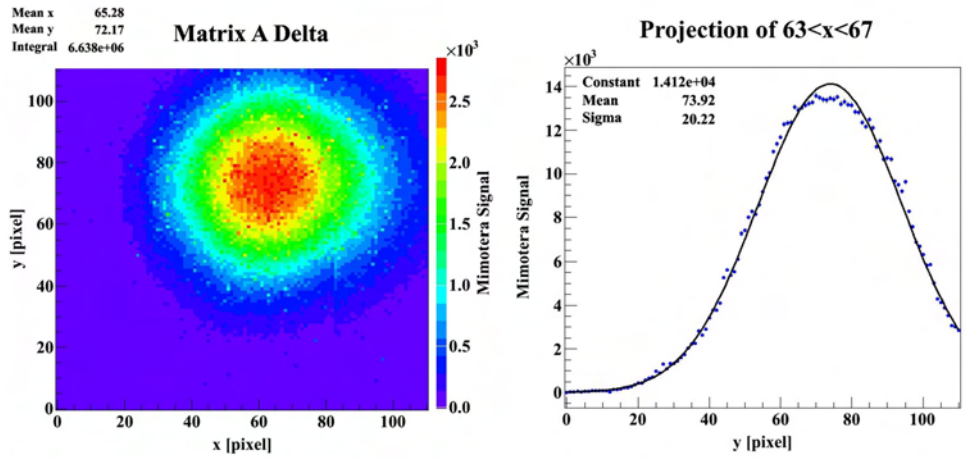

Figure 2: Profile of one shot of antiprotons in the *Mimotera*. Mean values in x- and y-direction are displayed, as well as the integral over the whole detector surface. The right picture includes a Gaussian fit.

Figure 2 shows the profile of one single beam spill in the *Mimotera*. The data matches well with the Gaussian fit displayed on the projection. The linearity of the detector can be specified by comparing the integrated signal in the *Mimotera* to the nominal beam intensity as given out by the accelerator log file. Without saturation in the sensor, the behavior should be linear with the number of particles. A deviation from linearity of less than 1 % has been observed, caused by saturation at the highest intensities in the very center of the beam in Figure 2. Reference measurements with gafchromic films result in the same sigma value.

4. Measurements at HIT

The *Mimotera* has not only been tested with antiprotons, but also with carbon ions at the Heidelberg Ion-Beam Therapy Center (HIT) in Heidelberg, Germany. The aim of these measurements was to investigate whether it could serve as a beam monitor for existing cancer treatment facilities. A scan through all available beam intensities from 5.0×10^6 s^{-1} to 8.0×10^7 s^{-1} has been performed, the results are presented in Figure 3.

The detector response is very good, clear beam spots were obtained from the lowest to the highest intensity. The behavior is linear within the uncertainties of the nominal beam intensity provided by the accelerator operation software. These measurements allowed concluding that the *Mimotera* is suitable for direct monitoring of carbon ion beams used in current heavy ion facilities.

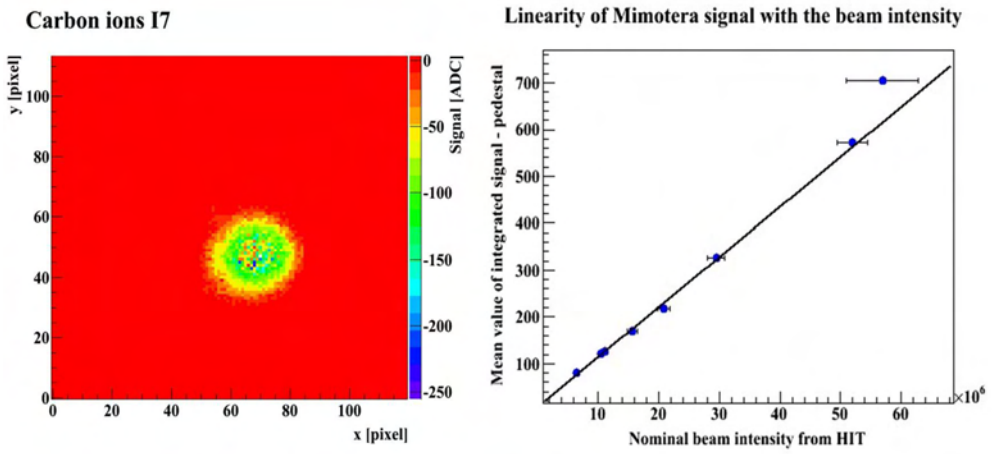

Figure 3: On the left: Profile of carbon beam integrated over two minutes. On the right: Linearity plot obtained from the intensity scan. The signal is averaged over the whole spill and background is subtracted.

It is, however, not applicable for proton beams at HIT at the moment, because the energy deposition per particle is too small for a good signal. Carbon ions of 410 MeV/n deposit 288 keV in 14 μm of silicon, in contrast to protons of 211 MeV which deposit only 12 keV. [5] Lower proton energies with higher ionization unfortunately could not be tested at HIT, because the focus size of the beam increases rapidly with decreasing energy, e.g. 32 mm minimum focus for 50 MeV protons.

5. Summary and Outlook

It has been shown that the *Mimotera* is well suited for direct monitoring of very short pulses of antiprotons as well as of continuous beams of carbon ions. Further investigation will focus on monitoring proton beams. To be able to monitor even larger focus sizes, one could merge four of the sensors together. To reduce the beam straggling further, such that the sensor could stay in the beam during treatment, it is possible to remove the PCB background behind the sensor.

Acknowledgments

The *Mimotera* architecture is protected by the U.S. patent no. 7582875, it was developed by the *SUCIMA* collaboration, with a project supported by the European Commission under the contract no. G1RD-CT-2001-00561.
This work was supported by the DFG under contract WE3565-3 and the NSF under grant # CBET 0853157. MHH acknowledges support by the EU through a Marie Curie Fellowship under contract # PIIF-GA-2009-234814.
Special thanks go to M. Caccia at Universita dell' Insubria, Como, for providing the detector and for much technical and scientific support, and to L. Negrini for being a great help in the data analysis.

References

[1] http://ptcog.web/psi.ch/
[2] T. E. Kalogeropoulos, R. Muratore; Nucl. Inst. Meth. B40/41 (1989) 1322-25.
[3] M. Holzscheiter et al.; Radiotherapy & Oncology, vol. 81, (2006) pp. 233-242.
[4] L.Bandano: Developpement d'un moniteur de faisceau innovant pour la mesure en temps reel des faisceaux utilises en hadron therapie. PhD thesis, 2005.
[5] http://www.sgeier.net/tools/bbt.html

Appendix II

Real Time Imaging of Antiprotons Stopping in Biological Targets – Novel Uses of Solid State Detectors

Stefan Sellner[a], Carsten P. Welsch[b], Michael Holzscheitera,[c]

[a]Max Planck Institute for Nuclear Physics, Heidelberg, Germany
[b]Cockcroft Institute, Warrington, UK
[c]University of New Mexico, Albuquerque, USA

Available online at www.sciencedirect.com
ScienceDirect
Radiation measurements 00 (2010) 1–4
Radiation measurements

Real Time Imaging of Antiprotons Stopping in Biological Targets – Novel Uses of Solid State Detectors

Stefan Sellner[a,*], Carsten P. Welsch[b], Michael Holzscheiter[a,c]

[a] *Max Planck Institute for Nuclear Physics, Heidelberg, Germany*
[b] *Cockcroft Institute, Warrington, UK*
[c] *University of New Mexico, Albuquerque, USA*

Abstract

Antiprotons have special properties which makes them possible candidates for particle beam cancer therapy. They behave nearly identical to protons in the entrance channel but deposit additional annihilation energy when they come to rest in the Bragg peak region. A significant part of this energy results in the creation of high energy pions. They exit the body mostly non-interacting and can be detected with an external detector, enabling a real-time supervision of the antiproton stopping distribution during irradiation process. This is currently not possible in any other particle treatment method.

In this contribution, the feasibility of using a silicon pixel detector in the Antiproton Cell Experiment (ACE) at the Antiproton Decelerator (AD) at CERN as well as simulations of the experiment for a more clinical environment are shown.

Keywords: silicon pixel detectors, particle beam therapy, medical imaging, antiproton annihilation

1. Introduction

Besides maximal tumor control, the ultimate goal of cancer treatment is to spare healthy tissue as much as possible from damage introduced by the therapy process. Current particle beam radiotherapy offers the possibility to deposit dose to tissue with a high degree of conformity, but treatment planning systems must rely on input data that are often not known precisely enough. For example, the conversion of Hounsfield values to material densities [1] and systematic errors in stopping powers introduce physics-related uncertainties. Together with small geometrical changes due to patient motion or change in patient anatomy, this can lead to a degradation of the desired depth dose distribution. To prevent unwanted dose deposition to healthy tissue, a method to detect and correct for such deviations in real time is necessary and desirable.

Several methods have been proposed for such a supervision of the irradiation process.

PET imaging: Positron emission tomography (PET) offers the possibility to confirm the treatment delivery in a non-invasive way by using the β^+ emitters created by nuclear interactions of the projectile ions with the surrounding target [2]. The created β^+ activity is correlated to the dose deposition. From the treatment plan, the expected β^+ activity is simulated and measured either after a treatment session in a full-ring PET scanner or in real-time using an

*Corresponding author. Tel.: +49 6221 516 421 Max-Planck-Institut for Nuclear Physics, Saupfercheckweg 1, 69117 Heidelberg, Germany
Email address: Stefan.Sellner@mpi-hd.mpg.de (Stefan Sellner)

in-beam PET device [2]. This method has been used successfully to verify or find deviations in the treatment plan [3]. However, it is not real-time, as even the in-beam method requires time to collect sufficient statistics.

Prompt gamma camera: A promising approach is to detect prompt gamma radiation released after nuclear fragmentation events. According to Testa et al. [4], ion ranges can be determined in real-time with an accuracy of about 1 mm. However, the signal to background ratio is currently only in the range of 3.

Apart from possible radiobiological benefits of radiotherapy using antiprotons [5, 6], secondary particles created by annihilation events, particularly charged pions, offer the opportunity to supervise the stopping distribution in real-time. Kantemiris et al. [7] have shown in simulations that the annihilation vertex distribution can be reconstructed with 1 mm precision. However, for that purpose they used a virtual high-end silicon pixel detector setup, consisting of 4 detectors with an active area of 40×40 cm^2 with three separate detection planes. In principle, such a set-up would allow to verify the agreement between the actual dose deposition and the treatment plan in the very initial fraction of the treatment, but the cost of the system would be prohibitive.

In this contribution, results from a pilot experiment of the Antiproton Cell Experiment (ACE) collaboration [8], where real-time imaging using a simple detector setup was investigated, are presented. Using a single detector plane set-up in an unconventional way facing the origin of the secondary pions with its edge, rather than with the front face, tracks of pions were observed in the detector. An analysis of the track length distribution alone allowed detection of the annihilation vertex distribution along the beam axis.

2. Methods and materials

The detector used is a spare ladder of 10 silicon pixel detector chips, which forms part of the vertex detector in the ALICE experiment at CERN. In total, it has 256×320 pixels, each with dimensions of 50 µm $\times$ 425 µm, and a thickness of 200 µm. In the experiment, this detector was mounted with the long edge (13.6 cm $\times$ 200 µm) perpendicular to the beam direction and slightly rotated around its vertical axis such that the long edge points towards the distal end of the water phantom (cf. figure 1).

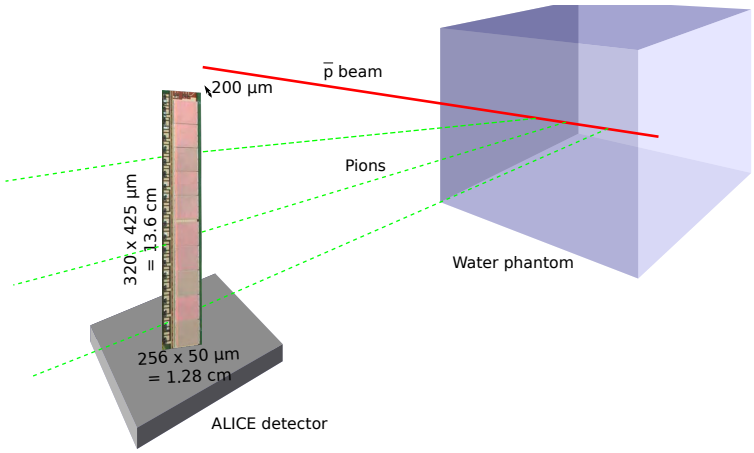

Figure 1: Experimental set-up

The dimensions of the phantom are $22 \times 22 \times 22$ cm^3. It was irradiated with 500 MeV/c antiprotons from the antiproton decelerator (AD) facility at CERN [9]. The AD cycle provides about 3×10^7 antiprotons in a 500 nanosecond pulse every 90 seconds. The detector properties allow a maximum occupancy of roughly 8 %, which was accounted for by placing it 1.4 meters away from the beam axis and setting the integration time to the last 100 ns of the antiproton pulse.

Secondary particles, especially pions, emitted by annihilation events along the incoming beam and in the stopping distribution at the end of range, enter the detector under an oblique angle. The angle with respect to the 1.28 cm side determines the length of the tracks the particles leave in the detector.

A track detection algorithm was developed to automatically identify the particle tracks. The length and position of the tracks are then back-calculated to reconstruct the annihilation vertex position along the beam axis.

To aid the interpretation of the data, simulations using FLUKA 2008.3c.0 [10] were performed. Here, the exact experimental set-up was modeled including all materials in the path of the primary beam, and the pixels traversed by the secondary pions were recorded. For statistics, 50 sets with 40 million particles each were used per run.

In the experiment, data was collected parasitically to the irradiation experiments and dosimetry tests of the ACE collaboration in 2009, providing about 100 individual spills.

To mimic a more realistic clinical environment, simulations were carried out for a continuous antiproton beam with much lower instantaneous intensity. As in this case, the detector could be located closer (30 cm) to the water phantom, the problem with the occupancy of the detector would not be present.

3. Results

The measured, as well as the simulated, annihilation vertex distributions are plotted in figure 2. The Bragg peak is located at 11 cm. In particular the measured annihilation vertex distribution is very broad. This is due to multiple scattering of the pions within the water phantom, which is magnified by the large distance between phantom and detector. As a consequence, the real distribution is blurred by a gaussian distribution with a FWHM of about 9 cm, leading to a long tail behind the distal end of the Bragg peak. Another effect is the imperfection of the line detection algorithm which was optimized to detect straight and clearly separated horizontal lines. The measured data, however, contains tracks that are due to secondary particles created from antiprotons that annihilated elsewhere, for example in the beam pipe, which deteriorates the line information. Nevertheless, the Bragg peak can be identified and matches the one obtained in the simulation.

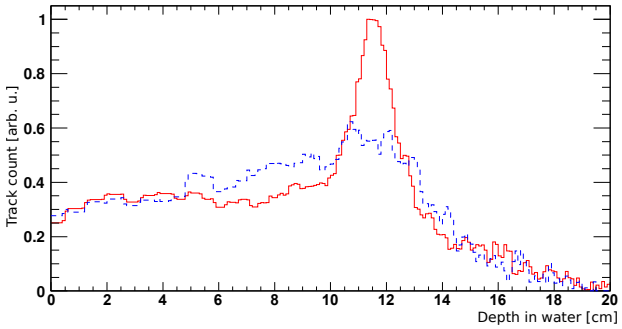

Figure 2: Measured (blue dashed line) and simulated (red solid line) annihilation vertex distribution along the beam axis

For the more clinical example, again 50 times 40 million antiprotons were simulated with the distance between the detector and the water phantom decreased to 30 cm. Here, the maximum of the differential antiproton fluence (green histogram in figure 3) coincides perfectly with the shoulder of the reconstructed annihilation vertex distribution (red line). Even more, the range of the antiprotons can be determined in the order of a few millimeters after the very first fraction of the irradiation as shown by the blue line, where the signal of only 10^8 antiprotons was evaluated. This corresponds to a dose of about 20 mGy in 10 mL water [6].

4. Discussion

The feasibility of imaging the stopping distributions during irradiation of a water phantom with antiprotons by tracking annihilation pions was demonstrated. In principle, this also holds for real-time imaging, which has however not been shown directly because of experimental limitations, due to the delivery modus of the Antiproton Decelerator consisting of bunches with long breaks in between. In simulations, however, it has been shown that the amount of incident antiprotons needed to obtain a reasonable signal is low compared to the amount which would be applied during one treatment fraction. The method to reconstruct the annihilation vertex distribution is to use the track information obtained by a silicon pixel detector, which is traversed by pions created in antiproton annihilation events. The

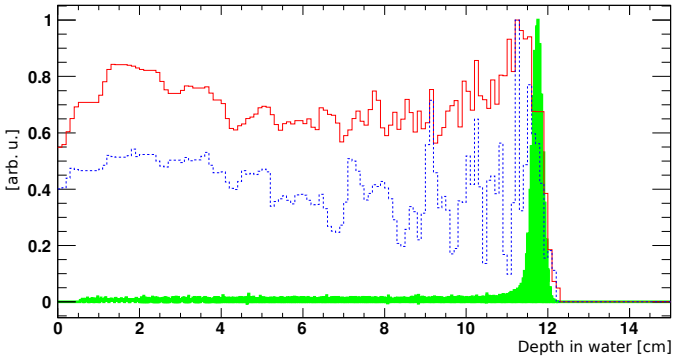

Figure 3: Simulation of a more clinical set-up: distance between water target and detector 30 cm. Red solid line: reconstructed annihilation vertex distribution (2×10^9 antiprotons), green filled in histogram: differential antiproton fluence, blue dashed line: reconstructed annihilation vertex distribution using only 10^8 antiprotons.

resolution in the experiment carried out was limited by the pion scattering in the water phantom, which was magnified by the large distance between detector and water phantom.

However, the limitations in this experiment would not exist in realistic clinical environments, as shown in simulations. There, it would be possible to use a more specialized detector with a sufficiently high resolution, which can be placed closer to the patient because of the much lower instantaneous beam intensity.

5. Acknowledgements

We would like to thank Petra Riedler, Vito Manzari, Michele Caselle and Michel Morel from the ALICE SPD group for their great interest in this field, for providing the detector, and for their support during the experiment. This work is supported by the EU through a Marie Curie Fellowship under contract PIIF-GA-2009-234814, the Helmholtz Association of National Research Centers (HGF) under contract number VH-NG-328, the GSI Helmholtz Center for Heavy Ion Research GmbH, by DFG under contract WE3565-3, and by the NSF under grant # CBET 0853157.

References

[1] O. Geiss, D. Schardt, B. Voss, M. Krämer, G. Kraft, Correlation between CT number and water equivalent thickness, GSI Report 99-01.
[2] K. Parodi, T. Bortfeld, T. Haberer, Comparison between in-beam and offline positron emission tomography imaging of proton and carbon ion therapeutic irradiation at synchrotron- and cyclotron-based facilities, Int. J. Radiat. Oncol. Biol. Phys. 71 (3) (2008) 945–956.
[3] K. Parodi, T. Bortfeld, W. Enghardt, F. Fiedler, A. Knopf, H. Paganetti, J. Pawelke, G. Shakirin, H. Shih, PET imaging for treatment verification of ion therapy: Implementation and experience at GSI Darmstadt and MGH Boston, Nucl Instrum Methods Phys Res A 591 (1) (2008) 282 – 286.
[4] E. Testa, et al., Dose profile monitoring with carbon ions by means of prompt-gamma measurements, Nucl Instrum Methods Phys Res B 267 (2009) 993–996.
[5] N. Bassler, I. Kantemiris, P. Karaiskos, J. Engelke, M. H. Holzscheiter, J. B. Petersen, Comparison of optimized single and multifield irradiation plans of antiproton, proton and carbon ion beams, Radiother Oncol 95 (1) (2010) 87–93.
[6] N. Bassler, J. Alsner, G. Beyer, J. J. DeMarco, M. Doser, D. Hajdukovic, O. Hartley, K. S. Iwamoto, O. Jäkel, H. V. Knudsen, S. Kovacevic, S. P. Møller, J. Overgaard, J. B. Petersen, T. D. Solberg, B. S. Sørensen, S. Vranjes, B. G. Wouters, M. H. Holzscheiter, Antiproton radiotherapy, Radiother Oncol 86 (1) (2008) 14–19.
[7] I. Kantemiris, A. Angelopoulos, N. Bassler, N. Giokaris, M. H. Holzscheiter, P. Karaiskos, T. E. Kalogeropoulos, the AD-4/ACE Collaboration, Real-time imaging for dose evaluation during antiproton irradiation, Phys. Med. Biol. 55 (2010) N1–N9.
[8] M. H. Holzscheiter, N. Bassler, N. Agazaryan, G. Beyer, E. Blackmore, J. J. DeMarco, M. Doser, R. E. Durand, O. Hartley, K. S. Iwamoto, H. V. Knudsen, R. Landua, C. Maggiore, W. H. McBride, S. P. Møller, J. Petersen, L. D. Skarsgard, J. B. Smathers, T. D. Solberg, U. I. Uggerhøj, S. Vranjes, H. R. Withers, M. Wong, B. G. Wouters, The biological effectiveness of antiproton irradiation, Radiother Oncol 81 (3) (2006) 233–242.
[9] S. A. Baird, D. Berlin, J. Boillot, J. Bosser, M. Brouet, J. Buttkus, F. Caspers, V. Chohan, D. Dekkers, T. Eriksson, R. Garoby, R. Giannini, O. Gröbner, J. Gruber, J. Y. Hémery, H. Koziol, R. MacCaferri, S. Maury, C. Metzger, K. D. Metzmacher, D. Möhl, H. Mulder, M. Paoluzzi, F. Pedersen, J. P. Riunaud, C. Serre, D. J. Simon, G. Tranquille, J. W. N. Tuyn, A. Van der Schueren, The antiproton decelerator: AD (CERN-PS-97-036-HP).
[10] A. Fassò, A. Ferrari, J. Ranft, P. Sala, FLUKA: A multi-particle transport code, CERN-2005-10.

Appendix III

Analysis of Antiproton induced DNA damage 2008-2010

Fred Currell, Joy Kavanagh, David Timson, Giuseppe Schettino

Centre for Cancer Research and Cell Biology, Queen's University, Belfast

Analysis of Antiproton induced DNA damage 2008-2010

Introduction

Radiotherapy employs ionizing radiation (IR) to cause lethal damage to tumour cells. It is widely accepted that cellular DNA is the most critical target. Immediately following an insult on DNA, damage-sensing proteins (e.g. 53BP1, ATM) are recruited to the site of damage. This signals cell cycle arrest so that DNA repair can take place [1], [2]. If the damage is too extensive to be repaired, cells may fail to perform "normal" functions and programmed cell death (apoptosis) can be initiated. Damaged cells whose cell cycle checkpoints have been compromised may not arrest and enter mitosis. This may result in cells producing progeny with a defective or abnormal genotype. The majority of those cells will experience mitotic catastrophe, a common phenotype of which is enlarged cells containing multiple micronuclei. Following a mitotic catastrophe, cells may continue to cycle for a short time but they are not viable long-term as they lack significant genetic information, and they will ultimately undergo cell death. This type of damage-induced response, called mitotic cell death, can be a mechanism by which cells prevents aneuploidy which can lead to tumorigenesis [3], [4]. A few "abnormal" cells can, however, survive and lead to long-term effects such as carcinogenesis. The micronucleus assay is commonly employed to determine levels of chromosomal damage in pharmaceutical and radiobiology research as well as clinically for staging of a number of cancers such as colorectal adenocarcinoma [5,6,7,8]. In addition to direct damage from IR, there is mounting evidence for the existence of a non-targeted effect in which non-irradiated cells respond to the damage of their neighbours. This effect is known as the radiation induced bystander effect (RIBE) and it has been demonstrated in vitro for a number of endpoints including clonogenic survival, histone H2AX phosphorylation (γ-H2AX) and genetic instability. There are also a number of in vivo studies showing these effects in mice. It is likely that RIBEs may contribute to the clinical appearance of abscopal effects post radiotherapy [9,10,11].

Aims

1. Quantify DNA damage in human cells along and around a 126 MeV antiproton beam at CERN.
2. Investigate immediate and longer term DNA damage.
3. Investigate non-targeted effects outside the beam path due to secondary particles or bystander signalling.

Overview of 2008-2010

The γ-H2AX and micronucleus assays are commonly used to study immediate and longer term DNA damage respectively. A pilot study at CERN in October 2008 demonstrated the applicability of this type of assay to studying antiproton induced DNA damage. Quantification of DNA double strand breaks/γH2AX foci in the nuclei of human fibroblast cells irradiated with antiprotons in 2009 revealed no significant increase in the number of foci present in SOBP irradiated cells when compared to those irradiated with the same dose in the plateau. Qualitative differences were however observed with significant clustering of foci in the nuclei of cells irradiated in the SOBP - a phenomenon not observed in plateau irradiated samples. The analysis

was performed 1hr post irradiation as it was aimed to determine the DNA damage induced. In planning for the 2010 AD4 beam time our main objective was to consolidate the data collected in previous years' beam times and extending our DNA analysis to 24 hrs post irradiation to investigate how cells were "processing" the radiation insults. The results from the quantification of micronuclei in cells irradiated in 2009 are consistent with the suggestion that plateau and SOBP damage is processed differently by the cells.

The physical set up designed for the 2009 beam time was employed also in October 2010.

Materials and Methods

Cell Culture

AG01522 human fibroblast cells were cultured in filtered alpha-MEM (LONZA, BioWhittaker®) supplemented with foetal bovine serum (15%), penicillin (100 IU/ml) and streptomycin (100 μg/ml) and HEPES buffer (25 mM) in a 95% air/5% CO_2 37^{o}C atmosphere. 10 h prior to treatment, cells were detached from culture flasks and were seeded in polystyrene slide flasks (NUNC) in 2 ml alpha-MEM and incubated. For the γ-H2AX assay ~6×10^5 cells seeded and for micronucleus assay ~ 3×10^4 cells seeded per sample. 2-3 h prior to irradiation sample flasks were filled with cold supplemented alpha-MEM (eliminating as much air as possible) and flasks were sealed closed. Samples were transported to CERN in an insulated container, maintaining the temperature at ~4 °C. Cell samples were kept cold for a maximum of 24 h. As cellular processes are considerably slower at 4 °C, cooling the samples is an established technique to minimize sample-to-sample differences due to dose rate and other experimental constraints.

Antiproton irradiation

Slide flasks containing cell samples were mounted within a phantom in specially designed holders. These were positioned at depths of 20 mm (plateau) and 101 mm (centre of SOBP). Cell samples were irradiated horizontally in an open water phantom with circulating water-glycerine mixture maintained at 4 °C. Cells received estimated antiproton doses in the plateau of 0.5, 1.0, 1.5 and 2.0 Gy. In addition to irradiated samples, control samples were mock irradiated and otherwise received the same treatment as irradiated samples.

Gafchromic film was attached to the back of all directly irradiated flasks so the treated area to be located post-treatment for analysis. DNA damage was scored in cells within an area 5mm in diameter at the centre of the region indicated by the Gafchromic films.

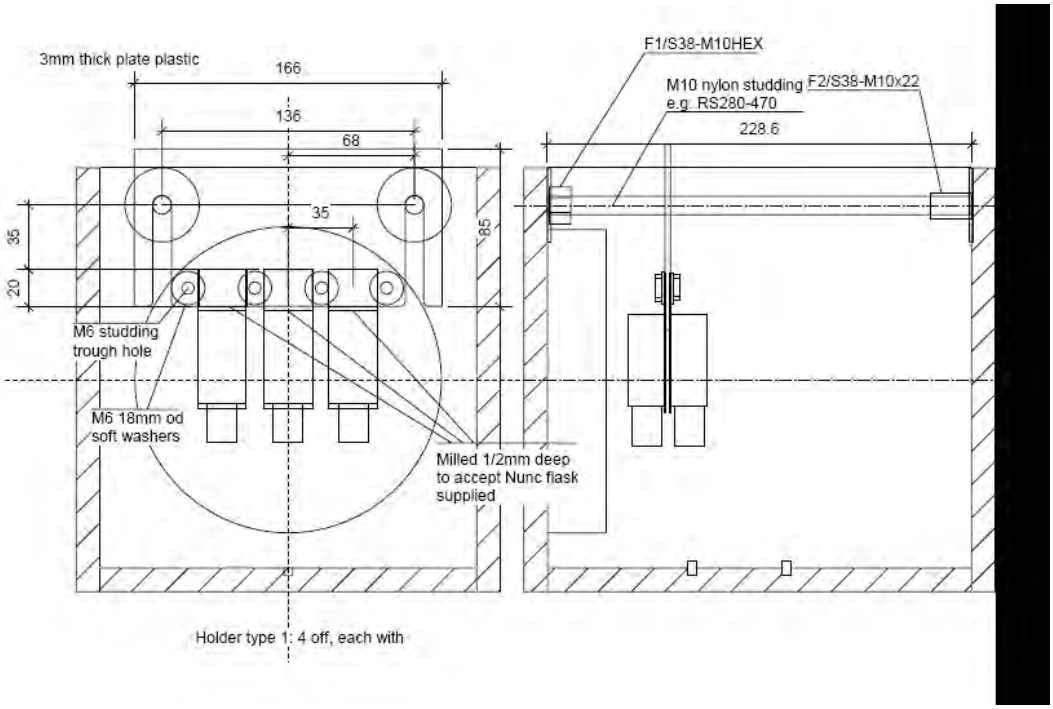

Fig.1. Experimental set-up for DNA damage experiments in 2009 and 2010. Cells were seeded for radiation in polystyrene slide flasks, which were aligned and fixed in position for irradiation with antiprotons. Schematic shows one sample holder as an example only. In the SOBP two flasks were fixed back-to-back as shown, cell monolayers separated by 3 mm within the SOBP.

Post radiation treatment

γ-H2AX assay

After the irradiation and upon arrival in the laboratory in University Hospital, Geneva, cold culture medium was aspirated from each slide flask and fresh, warm culture medium (4 ml) was promptly added to each flask. The flasks were subsequently incubated at 37 °C for 24 h after which time the cells were washed once with sterile PBS and fixed for 20 min with ice cold acetone:methanol.

Cells were permeablized with 0.5% Triton®X-100 (Sigma-Aldrich) solution in PBS for 20 min at 4 °C; non-specific binding was blocked with 0.2% skimmed milk, 5% foetal bovine serum and 0.1% Triton®X-100 in PBS for 1 h at 4 ºC. Cells were incubated for 1 h at 20 °C with anti-phospho-H2AX (mouse monoclonal antibody, clone JBW301, Upstate Biotechnology). Cells were washed in 0.1% Triton®X-100 solution and then incubated for 1 h at 4ºC with Alexa Fluor® 488 goat anti-mouse cross-absorbed antibody (Molecular Probes). Total nuclear DNA was stained with Hoechst stain. Slides were treated with Vectashield mounting media (Vector Labs) and covered with glass cover slips. Images were captured using a Zeiss camera. For directly irradiated samples, cell nuclei were scored only in the centre of the cover slip to ensure all cells within a scored sample had received uniform dose. Images of the cells show the nuclei stained blue and DNA damage (foci) shows up as bright green spots within the nuclei.

Micronucleus assay

1) Directly or secondary-particle irradiated samples were treated with cytochalasin-B (0.5µg/ml, Sigma) after 1 h incubation. These were incubated for a further 36 h (time at which maximum number of binucleated cells is seen in this cell line for this assay) at 37 °C prior to fixing. 2) Bystander cells were incubated for 1h with filtered culture media removed from directly irradiated samples prior to addition of cytochalasin B. The fixed cells were washed once in PBS and stored in fresh sterile PBS for transportation to Belfast.

Cells were stained with Acridine orange (Sigma, 25 µl/ml) for 20 minutes and washed with fresh PBS x5. Total nuclear DNA was stained with Hoechst stain. Samples were mounted and imaged as for γ-H2AX assay. The numbers of binucleated cells and binucleated cells which had micronuclei were scored within the beam diameter and outside of the beam (as determined with gafchromic film).

Cell survival assay

Post-treatment cell counting was performed for every sample and cells were plated in six well plates (Corning) at densities calculated to produce 50-60 colonies per well based on the estimated cell survival. 3 ml of fresh culture medium was added per well. The six plates were coded appropriately and subsequently incubated at 37 °C for 7-10 days. The colonies were fixed with methanol (Fluka, 2ml /well) for 15 min then stained with crystal violet (2%/70% methanol) for 60 min.

Statistical analysis

Non-parametric tests were carried out on data sets with non-Gaussian distributions. Data medians of treated sample sets were initially compared with Kruskal-Wallis non-parametric test, individual median values were compared using Dunn's multiple comparison test.

Results

Pilot experiment in October 2008

In 2008 human fibroblast monolayers which had been seeded in our laboratory in Belfast then flown to Geneva were irradiated. Despite having no sterile biological facilities in which to work at CERN we successfully irradiated a number of samples in the plateau and Bragg peak and also carried out media transfer experiments to investigate bystander signaling from antiproton irradiated cells.

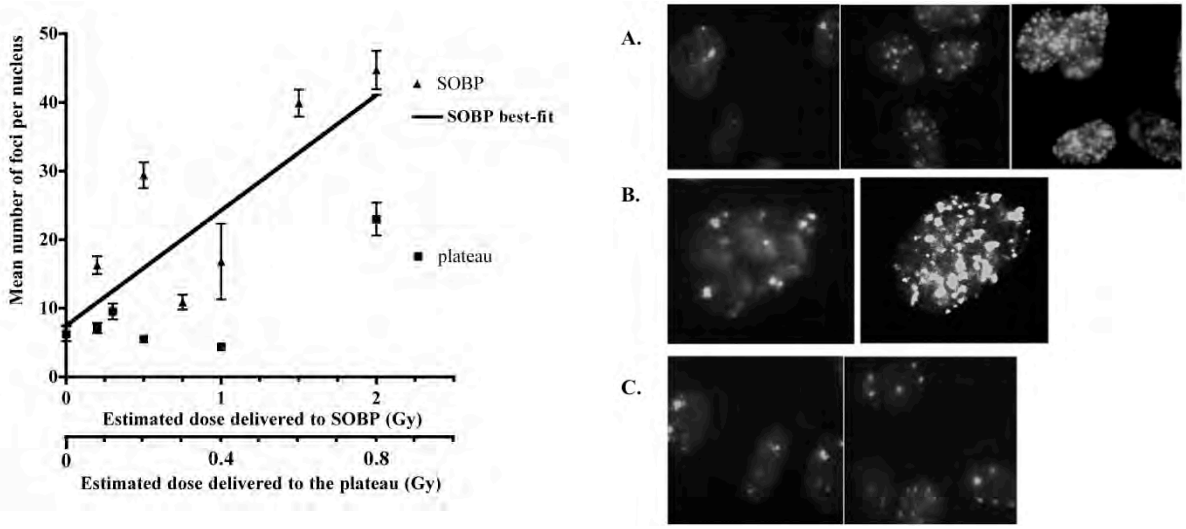

Fig.2. a) Antiprotons induced DNA double strand breaks in human fibroblast cells in a dose dependent manner. Phospho-H2AX foci were scored manually in the nuclei of 50 cells per dose point. Error bars indicate the standard error of the mean (SEM). b) Phospho-H2AX foci were observed by fluorescence microscopy. A) The frequency of foci was observed to increase in with dose. B) Cells irradiated in the SOBP (right) displayed large, clustered foci, which were not observed in plateau irradiated cells (left). C) cells positioned out side the beam (left) and media transfer treated cells displayed only minor increases in DNA damage compared to control samples.

This pilot data was presented at the RADAM meeting in Frankfurt during July 2009 and has subsequently been published in a topical issue of the European Physical Journal D [12].

2009 beam time

Building on the success of the 2008 beam time we implemented a number of changes to the physical set-up of our experiment to further enhance its potential to yield high quality data. In addition to this we were granted permission by Oliver Hartley to use his laboratory at the University Hospital Geneva during the beam times for set-up of our samples.

1. Antiproton Induced DNA damage

We were able to repeat the measurements that were made in 2008 for the γ-H2AX DNA damage assay.

a) b)

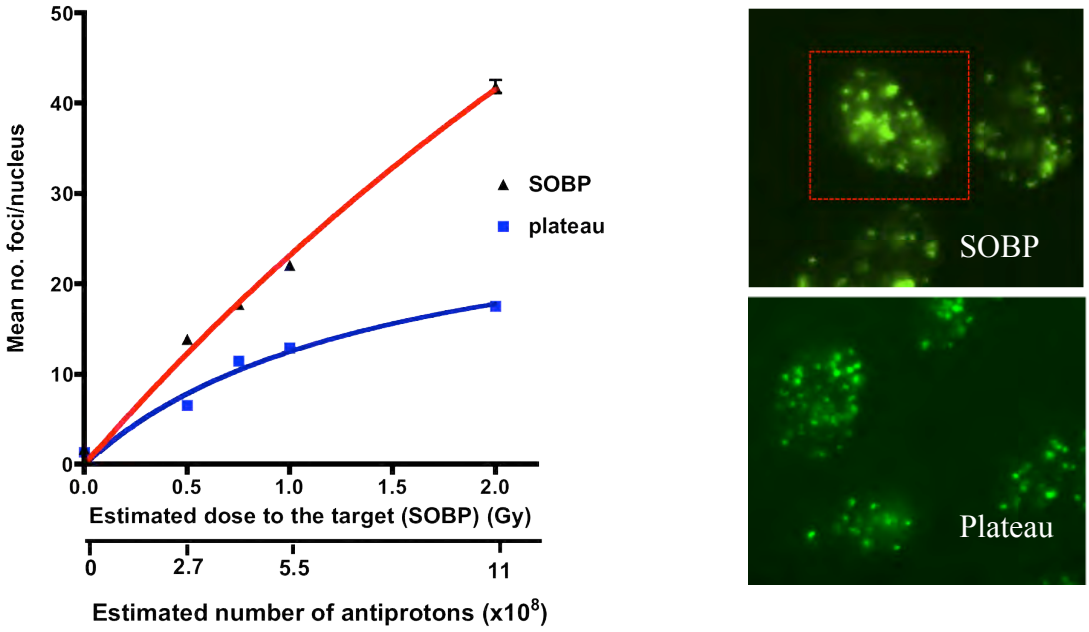

Fig. 3. Direct traversal of cells by antiprotons in low and high LET regions of the Bragg curve cause DNA damage. a) The graph shows the quantification of γ-H2AX foci in cells irradiated with up $1.1x10^9$ antiprotons in the plateau (blue) or SOBP (red) for each exposure. Foci were scored in at least 200 nuclei/sample and the means of at least two replicates are plotted for each dose point. Error bars indicate the SEM. The x-axis indicates the target dose of antiprotons delivered to cells in the centre of a SOBP. b) Representative images of fluorescent γ-H2AX foci in cells treated with antiproton SOBP (top) and plateau (bottom) are shown.

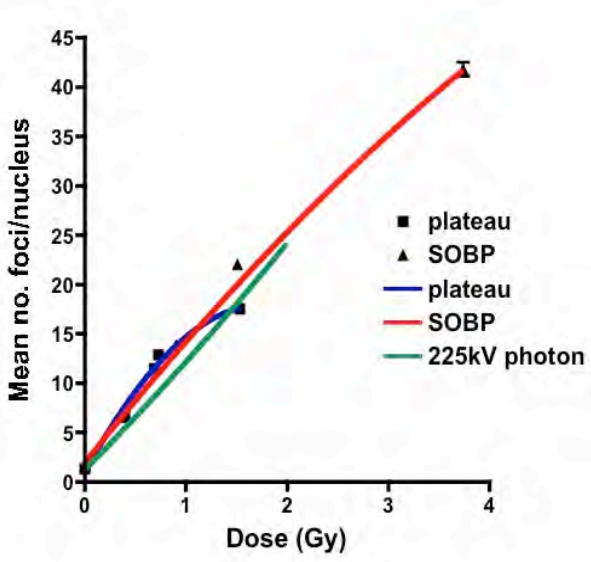

Fig. 4. Quantification of γ-H2AX foci induction 60 minutes after irradiation indicates no significant increase in RBE for antiprotons (peak) when compared to the same doses delivered by antiprotons (plateau) or by 225 kV X-rays (green).

Although no significant increase in the frequency of foci was detected in SOBP treated cells compared to plateau treated cells, for the same dose, a change in the size and shape of foci was observed (see also above.) The superior quality of data collected in the 2009 experimental session, allowed this variation in focus size to be quantified by comparing the FWHM (μm) for a random selection of foci in images of cells treated with antiprotons (peak and plateau) and conventional 225 kVp X-rays. This has revealed a highly significant increase ($p<0.0001$) in FWHM for antiproton (SOBP) treated cells compared to controls, X-rays and antiproton plateau irradiated cells. Data are shown in figure 5. There is no significant difference ($p>0.05$) in foci size for X-rays treated cells compared to antiproton plateau treated cells indicating a similar quality of damage induced. Damage produced in the SOBP area; however, produce considerably larger foci strong indication of an increase complexity of the insult.

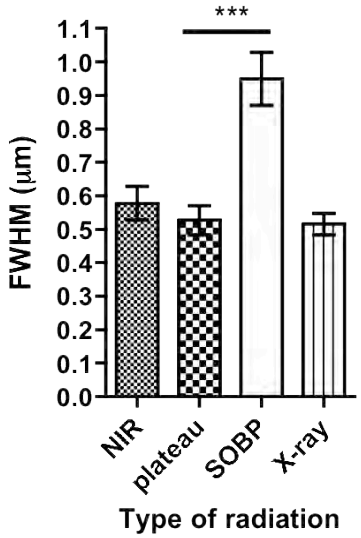

Fig. 5. Antiproton SOBP treatment induces larger DNA double strand breaks than either antiproton plateau or X-ray treatment. Mean FWHM of γ-H2AX foci in non-treated, antiproton plateau treated, antiproton SOBP treated and X-ray treated AG1522 cells are presented. At least 30 foci were selected at random from each sample type. *** indicates P value of less than 0.0001.

Non-targeted DNA damage induction

Out-of beam and off-target effects of radiotherapy are a cause of side effects. It is vital to understand the damage induced in cells outside of the target volume to enable the risk to normal tissues to be estimated. In contrast, if non-targeted effects, such as radiation induced bystander effects (RIBEs), are understood it may be possible in the future to manipulate these to achieve better therapeutic outcomes. We have positioned fibroblast cells adjacent to the Spread Out Bragg Peaks for each dose, but ~30 mm outside the beam path. As these samples are not in physical contact with irradiated cells but in the phantom at the time of irradiation, they will only experience scattered dose and secondary particles. On the other hand, in order to investigate the relevance of bystander signaling from antiproton treated cells we have transferred culture medium from antiproton SOBP treated cells onto naïve cells and then quantified the DNA damage response compared to control cells.

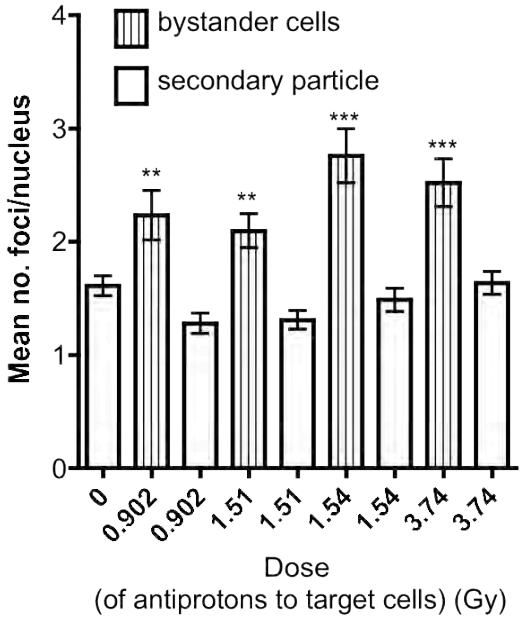

Fig. 6. Non-targeted effects of antiproton treatment. Foci were scored in at least 200 nuclei per sample. The data show the mean and SEM of at least two replicates for each dose point.

Within the dose range that we have been able to test thus far, no observable DNA damage has been observed in cells ~ 30 mm outside the beam path due to annihilation secondary particles (fig. 6). The dose from secondary particles in the range tested here is expected to be less than 10% of the in-beam dose to the target. Therefore future experiments will need much higher doses to determine the biological effects of those particles.

A small but significant increase in DNA double strand breaks was observed in cells treated with culture medium from SOBP irradiated cells. This response appears to be dose independent. Similar saturation in response to bystander signaling has been observed previously following low LET irradiations. Therefore this data would be consistent with a non-dependence on LET for bystander response in non-irradiated cells.

2. Sub-lethal effects induced in human cells by Antiproton treatment

Longer-term sub-lethal effects were measured by the appearance of micronuclei in cells, which had gone through one nuclear division. The micronuclei contain fragments of or whole chromosomes damaged by the treatment. Loss of genetic material could result in cell death or malignant transformation.

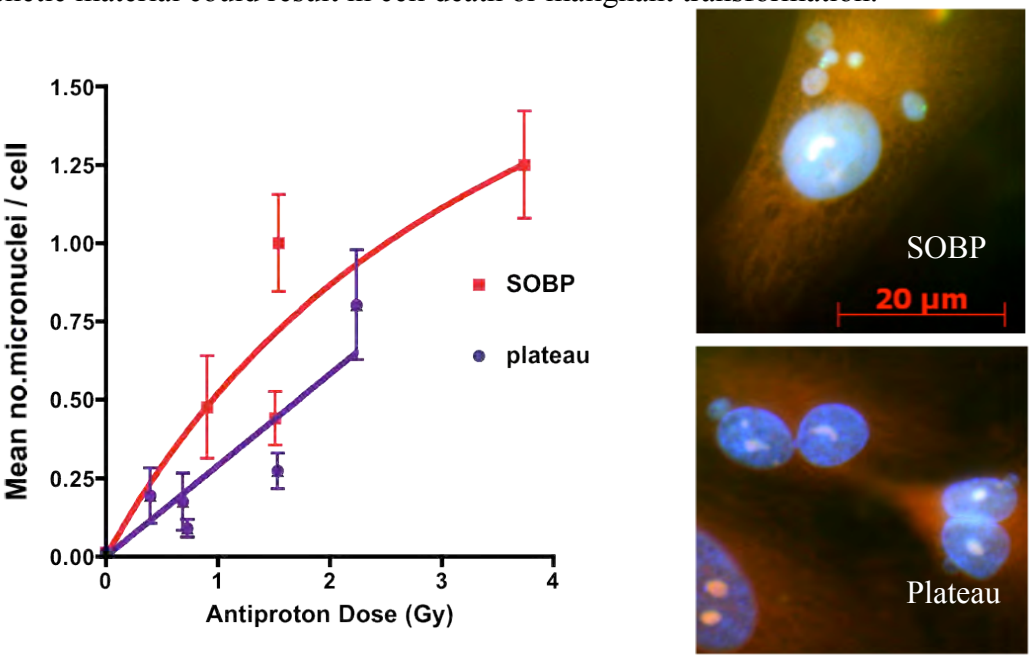

Fig. 7. 36 hours after treatment with antiprotons micronuclei are observed in cells which have undergone one nuclear division. The graph shows the mean and SEM of two replicate experiments and non-linear regression for the antiproton plateau and SOBP data sets. Representative images are shown (right) of cells for micronuclei.

X-ray comparison is planned to assess RBE for plateau and SOBP. These data, however, show how sub lethal damage induction is also LET dependent, a point that needs further consideration and investigation for all particle therapy approaches.

2010 beam time.

Due to the experimental sessions occurring late in the year and the long post-irradiation processing times, this report is mainly based on the 2009 data with samples from the 2010 experiments still being processed. Our initial plans for the AD4 beam time in October of 2010 were to:

- Extend our DNA damage studies to 24 hrs post irradiation in order to further investigate the different quality of DNA lesions produced in the plateau and SOBP and how cells respond to them.
- Repeat and extend the micronuclei experiments to validate previous results and widen the sub-lethal investigations to out of beam samples (i.e. secondary particle and bystander effect).
- Investigate possible use of plasmids as a fast (<2 hours) biodosimeter

As a result of a significant loss of beam time, more than one half of the planned experiments could not be carried out. In order to complement our previous experiments and to make the best use of the available time we irradiated human fibroblast cells in plateau, centre of the SOBP and outside the beam with plateau doses from 0-2 Gy. By culturing the cells for 24hrs post irradiation, the repair of DNA damage in these cells was then analyzed to investigate how the different complexity of damage (described earlier in this text) affect the cell's outcome.

Data analysis from these experiments is on going and will be available early in 2011.

References

1 P. E. Bryant, "Enzymatic Restriction of Mammalian-Cell DNA - Evidence for Double-Strand Breaks as Potentially Lethal Lesions," Int J Radiat Biol **48**, 55-60 (1985).

2 E. P. Rogakou, D. R. Pilch, A. H. Orr, V. S. Ivanova, and W. M. Bonner, "DNA double-stranded breaks induce histone H2AX phosphorylation on serine 139," J Biol Chem **273**, 5858-5868 (1998).

3 M. Castedo, J. L. Perfettini, T. Roumier, A. Valent, H. Raslova, K. Yakushijin, D. Horne, J. Feunteun, G. Lenoir, R. Medema, W. Vainchenker, and G. Kroemer, "Mitotic catastrophe constitutes a special case of apoptosis whose suppression entails aneuploidy," Oncogene **23**, 4362-4370 (2004).

4 L. Molz, Boohe, L.H., Young, P., Beach, D. , Genetics, 773-782 (1989).

5 A. Karaman, D. N. Binici, M. E. Kabalar, and Z. Calikusu, "Micronucleus analysis in patients with colorectal adenocarcinoma and colorectal polyps," World J Gastroenterol **14**, 6835-6839 (2008)

6 R. A. El-Zein, M. B. Schabath, C. J. Etzel, M. S. Lopez, J. D. Franklin, and M. R. Spitz, "Cytokinesis-blocked micronucleus assay as a novel biomarker for lung cancer risk," Cancer Res 66, 6449-6456 (2006)

7 K. Utani, Y. Kohno, A. Okamoto, and N. Shimizu, "Emergence of micronuclei and their effects on the fate of cells under replication stress," PLoS One 5, e10089 (2010)

8 M. Fenech, "The micronucleus assay determination of chromosomal level DNA damage," Methods Mol Biol 410, 185-216 (2008).

9 C. Mothersill and C. B. Seymour, "Mechanisms and implications of genomic instability and other delayed effects of ionizing radiation exposure," Mutagenesis 13, 421-426 (1998)

10 C. B. Seymour and C. Mothersill, "Relative contribution of bystander and targeted cell killing to the low-dose region of the radiation dose-response curve," Radiation Research 153, 508-511 (2000)

11 M. Mancuso, E. Pasquali, S. Leonardi, M. Tanori, S. Rebessi, V. Di Majo, S. Pazzaglia, M. P. Toni, M. Pimpinella, V. Covelli, and A. Saran, "Oncogenic bystander radiation effects in Patched heterozygous mouse cerebellum," Proc Natl Acad Sci USA 105, 12445-12450 (2008).

12 J.N. Kavanagh, F.J. Currell, D.J. Timson, M.H. Holzscheiter, N. Bassler, R. Herrmann, K.M. Prise,and G. Schettino, European Physical Journal D 60, 209-214 (2010).